SCUOLA DI DOTTORATO

UNIVERSITÀ DEGLI STUDI DI MILANO-BICOCCA

Department of School of medicine

PhD program in Neuroscience Cycle XXXIII

curriculum in experimental neuroscience

Generation and characterization of a zebrafish Pompe disease model to test the efficacy of 3-BrPA as a new therapeutic molecule.

Bragato Cinzia

Registration number 759520

Tutor: Dr. Renato Mantegazza

Coordinator: Prof. Rosa Maria Moresco

ACADEMIC YEAR 2019/2020

.

A mio nonno Dante.
Manchi. Sempre.

A Gian Luca,
la mia persona.

A Marina.
Agguerrita revisore
e mentore.

Abstract

Excess glucose is stored as glycogen in skeletal muscle and liver as an energy substrate readily available through the glycolytic pathway. Perturbation of glycolytic enzymes results in glycogen storage disorders such as Pompe disease (PD) or glycogenosis type II. PD is an autosomal recessive metabolic disease with an estimated incidence of 1:40000 live births. PD is due to a defect of the lysosomal enzyme acid α-glucosidase (GAA), or acid maltase, necessary for glycogen degradation. The spectrum of disease severity encompasses a broad continuum of clinical phenotypes ranging from the most severe “classic” form, characterized by early childhood onset, severe cardiomyopathy, rapidly progressive course and fatal outcome before two years of age, to an “intermediate” infantile form expressing a milder phenotype, and to juvenile and adult forms characterized by prevalent involvement of skeletal muscle. The almost total deficiency of the GAA enzyme results in the severe infantile form, while partial deficiency is responsible for the intermediate and mild forms. Enzyme replacement therapy (ERT), where GAA is provided via intravenous infusion is the only therapy available since 2006. While ERT represented a major milestone in the treatment of patients with Pompe disease and it has been shown to be efficacious in infantile severe PD, not all late onset cases respond equally well to this treatment. Therefore, the correction of the skeletal muscle phenotype in late onset cases is still challenging, revealing a need for more effective therapies. GAA difficulties in restoring muscle function have been ascribed to a concomitant altered autophagy, a key molecular mechanism that maintains cellular homeostasis and ensures correct macromolecule turnover in the cell. However, it remains unclear how autophagy is disrupted in PD, since it is yet unknown if an excessive acceleration or reduction of this process is present. Notably, this recent defective autophagy finding in PD has stimulated both a reassessment of the pathogenic mechanisms as well as the investigation of new therapeutic approaches, including search for adjunctive and alternative therapies

addressing both glycogen accumulation and autophagy. Among the small molecules to be explored for interfering with glycogen accumulation we have selected the Acid-3-Bromopyruvic (3-BrPA), an inhibitor of hexokinase (HK), which is a key glycolytic enzyme. In vitro and in vivo studies have reported this molecule to be an efficacious anti-tumor drug, in those tumor phenotypes in which cancer cells preferentially depend on glycolysis to produce adenosine triphosphate (ATP) for growth and proliferation. The anti-cancer property of this particular compound is due to its ability to inhibit glycolysis, by abolishing cell ATP production and consequently impeding the transformation by hexokinase of glucose into glucose-6- phosphate, and to trigger modulation of the autophagic process. Among the different hexokinase isoforms HKI, HKII, HKIII, and HKIV found in mammals, HKII is expressed at relatively high level only in skeletal muscle, adipose tissue, and heart.

The aim of this project was to use 3-BrPA, as an inhibitor of the key glycolytic enzyme HKII, to modulate glycogen incorporation into cells. We used zebrafish as in vivo model, in order to evaluate the effect of this specific molecule on the muscular system at subcellular detail. The demonstration of its role as HKII inhibitor and as an autophagy modulator, has created the basis for developing a new strategy to improve muscle function in PD patients.

Abstract (Italian)

Il glucosio in eccesso viene immagazzinato come glicogeno nel muscolo scheletrico e nel fegato come substrato energetico facilmente disponibile attraverso la via glicolitica.
Il malfunzionamento degli enzimi glicolitici provoca disturbi da accumulo di glicogeno come la malattia di Pompe (PD) o glicogenosi di tipo II. PD è una malattia metabolica autosomica recessiva con un'incidenza stimata di 1 su 40000 nati vivi. La malattia di Pompe è causata da difetti a carico dell'enzima lisosomiale acid α-glucosidasi (GAA) o maltasi acida, necessario per la degradazione del glicogeno. Lo spettro di gravità della malattia comprende diversi fenotipi clinici. Essi vanno dalla forma "classica" più grave, caratterizzata da insorgenza durante la prima infanzia, cardiomiopatia grave, decorso progressivo rapido ed esito fatale prima dei due anni, fino ad una forma infantile "intermedia" esprimendo un fenotipo più mite e forme giovanili e adulte caratterizzate dal coinvolgimento prevalente del muscolo scheletrico. La quasi totale carenza dell'enzima GAA causa la forma infantile grave della malattia, mentre la carenza parziale è responsabile delle forme intermedie e lievi. La terapia sostitutiva enzimatica (ERT), in cui l'enzima GAA viene fornito tramite infusione endovenosa è l'unica terapia disponibile dal 2006. Nonostante l'ERT abbia rappresentato una pietra miliare nel trattamento dei pazienti con malattia di Pompe, e abbia dimostrato di essere efficace nella forma infantile grave, non tutti i casi ad esordio tardivo rispondono ugualmente bene a questo trattamento. Pertanto, la correzione del fenotipo muscolare nei casi ad esordio tardivo è ancora ostica, mettendo in luce la necessità di trovare terapie più efficaci. Le difficoltà nel ripristino della funzione muscolare da parte della GAA esogena sono state attribuite ad una concomitante alterazione dell'autofagia. Il processo autofagico è un meccanismo molecolare chiave nel mantenimento dell'omeostasi cellulare, e assicura il corretto turnover delle macromolecole nella cellula. Tuttavia, non è chiaro quali siano le

modificazioni dell'autofagia nella malattia di Pompe, poiché non è ancora noto se sia presente un'accelerazione o una riduzione eccessiva di questo processo.

In particolare, la recente scoperta di un processo autofagico difettoso nella malattia di Pompe, ha stimolato sia una rivalutazione dei meccanismi patogeni della patologia, sia lo studio di nuovi approcci terapeutici, compresa la ricerca di terapie alternative mirate sia all'accumulo di glicogeno che all'autofagia. Tra le numerose molecole interessanti per il loro effetto di interferire con l'accumulo di glicogeno, abbiamo selezionato l'Acido-3-Bromopiruvico (3-BrPA), un inibitore dell'esochinasi (HK), il quale riveste un ruolo molto importante, essendo un enzima glicolitico. Studi *in vitro* e *in vivo* hanno riportato che il 3-BrPA è un efficace farmaco antitumorale, in particolare in quei tipi di tumori in cui le cellule, per crescere e proliferare, dipendono preferibilmente dalla glicolisi per produrre adenosina trifosfato (ATP). La proprietà anticancro di questo particolare composto è dovuta alla sua capacità di inibire la glicolisi. Essa abolisce la produzione di ATP da parte della cellula, impedendo di conseguenza la trasformazione da parte dell'HK del glucosio in glucosio-6-fosfato, e innescando successivamente la modulazione del processo autofagico. Tra le 4 diverse isoforme di esochinasi presenti nei mammiferi (HKI, HKII, HKIII e HKIV), si è visto che l'isoforma HKII è espressa a livello relativamente alto solo nel muscolo scheletrico, nel tessuto adiposo e nel cuore.

Lo scopo di questo progetto è quello di testare l'azione del 3-BrPA, valutandone gli effetti sia sul sistema muscolare sia a livello subcellulare, e per fare questo, è stato generato un modello malattia in zebrafish.

Dimostrare il ruolo del 3-BrPA, sia come inibitore dell'HKII, sia come modulatore dell'autofagia, servirà a creare le basi per lo sviluppo di una nuova strategia terapeutica per la malattia di Pompe.

Contents

Introduction 1
1.1 Pompe disease 1
1.1.1 Definition 1
1.1.2 Epidemiology 2
1.1.3 Pathogenesis and diagnosis 2
1.1.4 Clinical features and symptomatology 3
1.1.4.1 Classic infantile-onset Pompe disease (IOPD) 3
1.1.4.2 Non classic IOPD 3
1.1.4.3 Late-onset Pompe disease (LOPD) 4
1.1.5 Therapeutic strategies 4
1.1.6 Side effects of ERT in PD patients 4
1.1.7 Complications 5
1.2 Basics of autophagy 7
1.2.1 Macroautophagy 7
1.2.2 Microautophagy 7
1.2.3 Chaperone-mediated autophagy 8
1.2.4 Autophagosome biogenesis 9
1.2.5 LC3 10
1.2.6 Beclin 1 10
1.2.7 p62 11
1.2.8 Atg4 12
1.2.9 Atg7 13
1.2.10 ULK1 14
1.2.11 Lysosome 14
1.2.12 mTOR 16
1.2.13 AMPK 17
1.2.14 Autophagy in Pompe disease 19
1.3 Zebrafish (*Danio rerio*) 21
1.3.1 Genetics 21
1.3.2 Zebrafish and human diseases 22

1.3.3 Myogenesis in zebrafish 24
1.3.4 Behavioral tests 25
1.3.5 Gene knockdown technologies in zebrafish 26
1.4 Acid 3-Bromopyruvic 27
1.5 Aims of the study 29
Glycogen storage in a zebrafish
Pompe disease model is reduced by 3-BrPA treatment 30
2.1 Abstract 30
2.2 Abbreviations 31
2.3 Introduction 32
2.4 Materials and Methods 35
2.4.1 Animal care 35
2.4.2 RNA extraction and reverse transcription 35
2.4.3 Morpholino injections 36
2.4.4 Western Blot 36
2.4.5 Yolk removal 38
2.4.6 Glycogen Assay 38
2.4.7 Embryo morphological characterization 38
2.4.8 Periodic acid–Schiff (PAS) staining 39
2.4.9 LysoTracker Red dye staining 39
2.4.10 Glycogen visualization with 2-NBDG 39
2.4.11 Quantification 40
2.4.12 qRT-PCR 41
2.4.13 *gaa* mRNA injection 42
2.4.14 3-BrPA treatment 43
2.4.15 Screening for embryonic motility 43
2.4.16 Data Analysis 44
2.5 Results 45
2.5.1 Characterization of the model 45
2.5.1.1 Zebrafish *gaa* gene 45
2.5.1.2 *gaa* knocked-down embryos displayed phenotypic defects and increased glycogen content 46
2.5.1.3 Morphological features were altered in *gaa* knocked down embryos muscle and heart 49

2.5.1.4 Lysosomal content was more increased in ATGgaa than in I9E10gaa morphants 49
2.5.1.5 Motility was defective in *gaa* knocked down embryos 51
2.5.1.6 Expression of autophagy-related transcripts and proteins was altered in I9E10*gaa* morphants 52
2.5.1.7 *gaa* mRNA injection rescued Pompe disease phenotype in I9E10*gaa* morphants 55
2.5.2.1 3-BrPA enhanced motility behavior in *gaa* morphants 58
2.5.2.2 3-BrPA improved muscle morphology in morphants 59
2.5.2.3 3-BrPA increased lysosomal content in morphants 60
2.5.2.4 3-BrPA treatments improved rescue in I9E10*gaa* morphants . 62
2.5.2.5 3-BrPA treatment modified the expression of *Beclin1, p62*, and *Lc3b* transcripts and proteins 65
2.6 Discussion 67
Conclusions 61
3.1 Zebrafish transient model and novel therapies for Pompe disease 61
3.2 Future prospects 62
3.3 Ongoing project on zebrafish transient PD model 64
3.4 Behind the 3-BrPA project 65
Bibliografy 66

1

Introduction

1.1 Pompe disease

1.1.1 Definition

In 1932 the Dutch pathologist Johannes Cassianus Pompe reported his findings in a 7-mont-hold girl who died presenting hypertrophic cardiomyopathy. At microscopic level, he found a large amount of glycogen accumulation in the heart, liver, kidneys and skeletal muscles. The disease, later classified as glycogen storage disease type II, was named after him thanks to his discovery [1].

In 1955 the Belgian cell biologist Christian de Duve and colleagues published a paper in which they described the lysosome, a subcellular-membrane-bound organelle that contains an array of enzymes capable of breaking down waste materials and cellular debris [2]. Such important discovery paved de Duve way to the Nobel Prize in Physiology and Medicine in 1974. This allowed acid α-glucosidase to be identified and studied by Henri-Géry Hers in 1963 [3]. Hers related the deficiency of acid α-glucosidase to five patients with Pompe disease infantile onset, letting Pompe disease became the first lysosomal storage disorder with a known cause.

During the following two decades, patients with varied age presenting acid α-glucosidase (GAA) deficiency with lysosomal glycogen increment were described. In 1970 Andrew Engel suggested the name acid maltase deficiency to make a distinction between patients with onset of symptoms in infants, late childhood or adulthood [4-6].

1.1.2 Epidemiology

The estimated incidence of GAA deficiency is reported as 1 in 40,000 born alive. The predicted incidence based upon carrier frequencies is reported as 1 in 138,000 for classic infantile disease and 1 in 57,000 for late-onset disease. Two different studies reported strategies for newborn screening (NBS) in Austrian and United States populations. They found a higher incidence (1 in 8686 and 1 in 21,979, respectively) for the early- and late-onset forms combined [7,8].

1.1.3 Pathogenesis and diagnosis

Pompe disease (PD), also known as Glycogen Storage Disorder Type II (GSD II), is a rare, inherited and often fatal autosomal recessive metabolic disorder (OMIM #232300). It is caused by mutations in a gene that is responsible of the enzyme, called acid alpha-glucosidase (GAA), production. The body uses GAA to break down glycogen, a stored form of glucose used for energy. The enzyme performs its function in intracellular compartments, the lysosomes. Alongside with autophagosomes, these organelles are known to function as cellular clearinghouses. In fact, the autophagosomes ingest multiple substances including glycogen, which is converted by the GAA, present in the lysosomes, into glucose, a sugar that fuels muscles. In Pompe disease, mutations in the *GAA* gene reduce the functionality of this essential enzyme. Increased quantity of glycogen accumulates throughout the body, but the cells in heart and skeletal muscles are the most affected. Currently, up to 600 different mutations in the *GAA* gene, which are the cause of Pompe disease symptoms, are identified. Both the severity of the disease and the age of onset seem to be related to the enzyme deficiency amount.

A diagnosis of Pompe disease can be confirmed by screening for the common genetic mutations or measuring the level of GAA enzyme activity in a blood sample. Once Pompe disease is diagnosed, testing of all family

members and a consultation with a medical geneticist are recommended. Carriers are most reliably identified via genetic mutation analysis.

1.1.4 Clinical features and symptomatology

The spectrum of disease severity encompasses a broad continuum of phenotypes ranging from the most severe “classic” form, characterized by child onset, severe cardiomyopathy, rapidly progressive course and fatal outcome before two years of age, to the “intermediate” infantile form with milder phenotype, to the juvenile and adult forms with prevalent involvement of skeletal muscle [9]. The almost total deficiency of the enzyme results in the severe infantile form, while partial deficiency is responsible for the intermediate and mild forms [10,11].

1.1.4.1 Classic infantile-onset Pompe disease (IOPD)

IOPD is the most severe form, characterized by the age of onset at ≤ 12 months, rapidly progressive hypertrophic cardiomyopathy, left ventricular outflow obstruction, hypotonia and muscle weakness, respiratory distress, and progressive loss of independent ventilation. Moreover, breathing difficulties, feeding problems, and macroglossia are reported. Motor development is significantly delayed, and major developmental milestones, such as the ability to roll over, sit, or stand, are often not achieved. Only a small percentage of untreated patients survive beyond 1 year of age; the main cause of death is cardiac and respiratory failure [12].

1.1.4.2 Non classic IOPD

This is the form in which patients that present similar clinical presentations of classic IOPD during their first year of life, with a minor cardiomyopathy and absence of left ventricular outflow obstruction are included. If untreated, severe muscle weakness will occur, leading to respiratory failure by early childhood [12].

1.1.4.3 Late-onset Pompe disease (LOPD)

LOPD is the less devastating form, and can occur any time after 12 months of age, usually without significant cardiac involvement. Late-onset patients commonly present the symptoms of proximal limb-girdle myopathy.

The symptoms progression is relatively slow but conclusively leads to profound muscle weakness and wasting, wheelchair dependency, and respiratory failure due to the involvement of the diaphragm [12].

1.1.5 Therapeutic strategies

Currently, the only approved therapy for PD patients is the Enzyme Replacement Therapy (ERT). ERT is based on the intravenous (IV) infusion of the recombinant human α-glucosidase (rhGAA). The uptake of this exogenous lysosomal enzyme is depending on the mannose-6-phosphate (M6P) receptors, present in muscles and liver [13].

In 1964, Christian de Duve was the first to suggest the replacement of the defective enzyme with a recombinant human enzyme, in order to restore the disrupted activity [14].

During the development of enzyme therapy, the production of rhGAA was tested at the same time in genetically modified Chinese hamster ovary cells and milk of transgenic animals. Finally, the production of rhGAA in milk of transgenic rabbits being chosen [15].

Pompe disease patients should be treated with ERT as earlier as possible during childhood, or when the symptoms appear during adulthood. The treatment is a lifelong therapy, which is not stopped or interrupted even if negative side effects occur.

1.1.6 Side effects of ERT in PD patients

ERT presents several side effects in patients, due to the needle infusion reaction or to the fluids involved in the intravenous delivery of the enzyme. The fluid infusion can be responsible of electrolyte problems, and the body may respond with swelling and irritation around the injection site or a more general fever. Furthermore, individual response to ERT is heterogeneous and influenced by many factors such as age at treatment initiation,

genotype, cross-reactive immunological material (CRIM) status, high and sustained antibody titers, causing allergic immune reaction to the enzyme itself, and IgE-mediated hypersensitivity reactions that may cause anaphylaxis [http://atm.amegroups.com/article/view/25969/24400].

Some patients have indeed reported the following reactions: allergic symptoms, including hives, a rash, fever, or life-threatening anaphylaxis; flushed skin, feelings of excessive heat or cold, and chills; low oxygen in the blood, resulting in pale, bluish, or purple skin; quickened heart rate and rapid breathing; headache, dizziness, or fainting; chest discomfort; high or low blood pressure; muscle tremors, pain, or fatigue; nausea and vomiting.

Moreover, in order to treat Pompe disease, higher doses of α-glucosidase enzyme are required, if compared to other diseases treatment, increasing the risks of the reported side effects.

1.1.7 Complications

The intravenous (IV) administrations of approved enzymes in Pompe disease generally represent a significant benefit at clinical level. In fact, improved walking ability, ameliorated respiration, lowering nocturnal apneas and improved life-quality are reported, although some residual mild weakness is present in treated patients.

ERT is not a cure for PD, and this pathology require repeated and life-long treatment for optimal clinical outcomes. Therefore, the cost-effectiveness and accessibility to ERT should be taken into consideration. Unfortunately, due to the high-cost of ERT (usually US $ 200.000/patient per year), it is not often accessible for countries with fewer resources [14]. Nowadays, the ERT is produced by Sanofi Genzyme company, marketed under the brand name Myozyme in Europe, and Lumizyme in the U.S. [16].

Despite ERT represents a major milestone in the treatment of patients with PD, and it has been shown to be efficacious in infantile severe PD, not all late onset cases respond equally well to this treatment. Therefore, the correction of the skeletal muscle phenotype in late onset cases is still challenging, revealing a need for more effective therapies [9,10,17-20]. rhGAA difficulties in restoring muscle function have been ascribed to a

concomitant altered autophagy, a key molecular mechanism that maintains cellular homeostasis and ensures correct macromolecule turnover in the cell. However, it remains unclear how autophagy is disrupted in PD, since it is yet unknown if an excessive acceleration or reduction of this process is present. Notably, the finding regarding the defective autophagy in PD has stimulated both a reassessment of the pathogenic mechanisms as well as the investigation of new therapeutic approaches, including search for adjunctive and alternative therapies addressing both glycogen accumulation and autophagy.

1.2 Basics of autophagy

Autophagy is a catabolic process involved in cellular homeostasis, and It is required to maintain normal cellular physiology under stressful conditions [21]. Autophagy is a selective or non-selective lysosomal degradative process, activated by different conditions via regulatory signaling complexes [22]. Autophagy acts as a cleaning mechanism by removing or degrading unnecessary materials from the body (e.g., proteins, organelles, and microbes) and retaining or maintaining materials (biochemicals, metabolites, and organelles) required for survival, function, and development. Three types of autophagy are known: macroautophagy, microautophagy, and chaperone-mediated autophagy (CMA) [23].

1.2.1 Macroautophagy

Macroautophagy, referred to "autophagy" in this thesis, is the major pathway which engulfs large portions of cytoplasm and cellular contents (i.e., long-lived proteins, aggregated proteins, damaged organelles, and intracellular pathogens) into a double membrane delimited vacuole called the autophagosome which, after fusion with lysosomes, forms the autolysosome. Successively, it degrades the autolysosomal contents, and recycles macromolecules for reuse [24,25].

Macroautophagy can be selective or nonselective [26,27]. The selective macroautophagy is characterized by tight interaction that are formed between the selected cargo and the growing phagophore. Contrarily, the nonselective or bulk macroautophagy is characterized by the inner surface of the growing phagophore which is not connected to any specific cargo, even if grows out from the ER as in selective autophagy [28].

1.2.2 Microautophagy

Microautophagy is the process by which lysosomes directly engulf and digest small volumes of cytosolic substrate [29]. Microautophagy takes place during the biogenesis of multi-vesicular bodies (MVBs). MVBs deliver to the late endosomes soluble proteins, and relies on electrostatic

interactions between endosomal sorting complexes required for transport (ESCRT I and III) and the heat-shock protein 70 (HSC70). For this reason, microautophagy involves both endocytic and autophagic components [23].

1.2.3 Chaperone-mediated autophagy

Chaperone-mediated autophagy (CMA) is induced by physiological stresses such as prolonged starvation [30]. The CMA pathway delivers target proteins across lysosomal membranes into the lysosomal lumen by interacting with lysosome-associated membrane protein type 2A (LAMP-2A) [24]. Hence, CMA differs from microautophagy and macroautophagy, as it does not require vesicular trafficking [30].

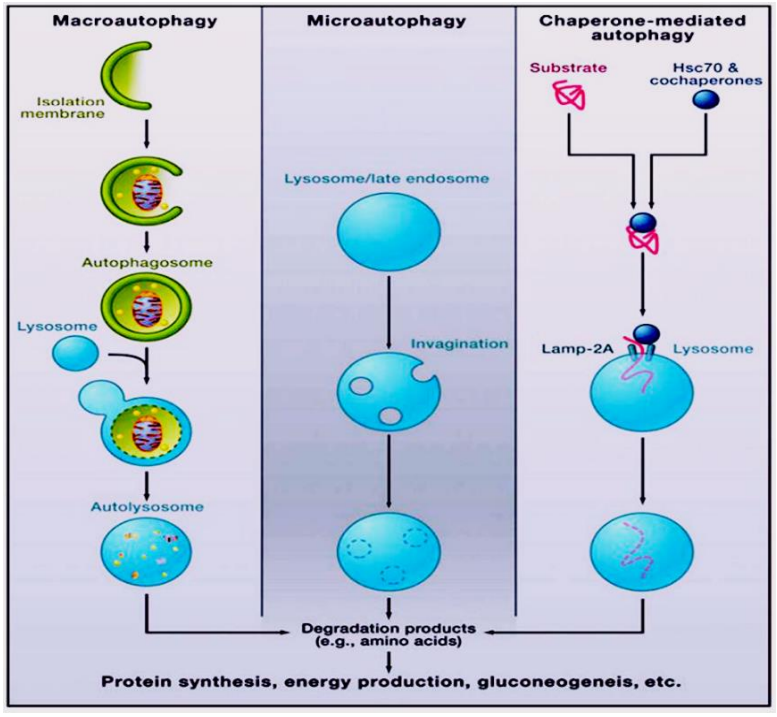

Fig. 1.2 *Different types of autophagy (cite from Mizushima N, Komatsu M. Cell 2011;147(4) 728-741).*

Numerous cellular regulators (e.g., transcription factors and genes) govern the physiological processes of every type of autophagy. They can affect homeostatic processing if disturbed by genetic or functional reasons. Hence, autophagy defects can be the pathogenic cause of many diseases. The roles of autophagy have been studied and related to health, disease,

infection, degeneration, and genetic or lifestyle-acquired diseases; nonetheless, cancer, microbial infections, and degenerative diseases [23]. Currently, the roles of autophagy are being the researching focus of diverse fields of study.

1.2.4 Autophagosome biogenesis

The autophagosomes are membrane-bound organelles generated de novo during the intracellular process of macroautophagy. Before bending into spherical double-membrane organelles, autophagosomes grow as flattened double-membrane sheets, called phagophores. During their life cycle, occurs a complex remodeling of the autophagic membrane, involving a multistep process which changes the morphology of the autophagic membranes.

The redesign of early autophagic membranes, and how they start their growth, is still under debate [31].

What is sure, is that the autophagy pathway begins when the phagophore born and ends when the autophagosome dies [32].

The autophagosome formation involves the ATG proteins, a dedicated cohort of proteins which assembles into functional complexes. They are activated and recruited to membranes to initiate autophagy. Among these proteins are present: the ULK complex, a serine-threonine kinase complex (ULK1, ULK2, ATG13, RBCC1/ FIP200 [RB1-inducible coiled-coil protein 1], ATG101); the class III lipid kinase complex I producing phosphatidylinositol-3-phosphate (PIK3C3/VPS34, PIK3R4/p150, BECN1/Beclin 1, ATG14); the effector of phosphatidylinositol 3-phosphate (PtdIns3P), the WIPI proteins; 2 ubiquitin-like conjugation complexes, one which conjugates ATG12 to ATG5 in association with ATG16L1 (ATG7, ATG10) and one driving the lipidation of the Atg8 family members (ATG7, ATG3). The Atg8 family in mammals consists of at least 6 proteins (LC3A, B and C, GABARAP. GABARAPL1, and GABARAPL2/GATE-16). There is only one transmembrane protein in this cohort, called ATG9, which has a still not a determined function, despite its recognized essentiality [32].

In this thesis, we observed changes in the expression level of some of these proteins, known to be related to the modulation of the autophagic process.
In particular, we observed ATG8/LC3 (Atg8-PE/LC3 II), in order to measure the levels of membrane-bound formation [33]. Furthermore, we observed SQSTM1/p62, a substrate of autophagy, Beclin 1/ATG6 and ATG7, which are components of the core autophagic pathway, and ATG4, the sole protease protein, which operate as an essential factor in the Atg8 conjugation system, one of the unique mechanisms in autophagy [34].

1.2.5 LC3

The microtubule-associated protein 1 light chain 3 (LC3 or GABARAP) was identified by the Dr. Yosimori group as a mammalian homologue of Atg8 [35].
LC3, the most studied family protein, is associated with autophagosome development and maturation and is used to monitor autophagic activity.
All along the formation process of autophagosomal membranes, the cytosolic LC3, called LC3-I, is conjugated to phosphatidylethanolamine (PE) through two consecutive ubiquitylation-like reactions. These reactions are catalyzed by the E1-like enzyme Atg7 and the E2-like enzyme Atg3 to LC3-II. During the fusion of autophagosomes with lysosomes, intra-autophagosomal LC3-II is degraded by lysosomal proteases. Modifications in cellular LC3-II level are connected to the dynamic turnover of LC3-II via the lysosome. LC3-II is synthesized by multiple processes, including C-terminal cleavage, and then can be affirmed that the LC3-II level reflects the number of autophagosomes.
Monitoring LC3-I and LC3-II expression is fundamental for the autophagy mechanism investigation [36].

1.2.6 Beclin 1

Beclin 1 was discovered in 1999 by the Dr. Beth Levine's group as the first mammalian autophagy-related gene, the mammalian homologue of yeast atg6 [37].

The discovery of Beclin 1 was strictly related to the finding of the anti-apoptotic protein B cell lymphoma-2 (Bcl-2), a member of the Bcl-2 family proteins.

The Bcl-2 gene was first discovered in the chromosomal translocation breakpoint of B cell follicular lymphoma [38], and was found that its overexpression prevents cell death.

While exploring the molecular mechanism responsible for this observation, the Levine group identified a new 60 kDa coiled-coil Bcl-2-interacting protein, which was named Beclin ("in" suffix, because it has a coiled-coil domain, and "Becl", because interacts with Bcl-2) [39].

Successively was found that Beclin 1 interacts not only with Bcl-2 but also with Bcl-xl and that the interaction site is present in the 262–450 aa of the Beclin 1 protein.

It is reported that Beclin 1 regulates autophagy by forming complexes with different proteins, as Class III PI3K [31].

PI3K is a family of enzymes that phosphorylate the 3'-hydroxyl group on the inositol ring of phosphoinositide. It regulates many physiological functions by producing phosphorylated phospholipids, that are signaling molecules including PtdIns(3,4,5) triphosphate and PtdIns(3,4) diphosphate. PI3K is widely involved in intracellular signal transduction pathways, and is mainly divided into three classes: I, II and III.

Class III PI3K phosphorylates PtdIns as a substrate to produce PtdIns(3) monophosphate.

Beclin 1 regulates autophagy forming complexes with different proteins, as Vps34, p150, Atg14 and UVRAG.

1.2.7 p62

Sequestosome 1 (SQSTM1)/p62/A170 or ZIP3 (hereafter referred to p62) is a stress-induced 62-kDa protein expressed in almost all the tissues. It is encoded by an immediate-early response gene activated by a variety of extracellular signals. These signals are involved in cell proliferation, differentiation and oxidative stress [40].

p62 is a multifunctional protein. One of its roles is to be a scaffold or adapter protein. In fact, p62 contains a series of motifs which enable its interaction with a profusion of selective signal transduction pathways, which are involved in cell proliferation and survival or death through regulation of transcription factor activities [41].

Furthermore, p62 acts as an autophagy receptor acting through three different and essential interactions.

First, p62 interacts directly with selected cargoes. p62 uses its C-terminal UBA domain to interact with ubiquitinated or non ubiquitinated cargoes. Second, it interacts with ATG8s anchored via their lipid tail to the inner membrane of the phagophore. Third, homopolymerization of p62 mediated by its PB1 domain facilitates its aggregation with the cargo. Polymerization also enables a tight interaction of the p62-coated cargo with lipidated ATG8s at the phagophore [28].

In 2016, studies by Dr. Weiguo Zhu and Ying Zhao at Peking University unveiled that accumulated p62 in autophagy-deficient cells directly binds to and inhibits histone ubiquitination, resulting in DNA damage [31].

During autophagy, p62 enables mTORC1 activation on lysosomes, possesses LC3-interacting region and can act as a cargo receptor for the autophagy of ubiquitinated proteins aggregated into p62 bodies [42].

Moreover, p62 is itself a substrate for selective autophagy and is often used as a marker of autophagic flux, as its accumulation can indicate inefficient (or blocked) autophagy [43,44].

p62 is involved also in the signalling pathways that control inflammation and is considered a crucial factor in the inhibition of inflammasome activity through its participation in autophagy enabling its degradation [28].

1.2.8 Atg4

Atg4 was originally identified in budding yeast as a sole cysteine protease specific to Atg8. Together with Atg8, Atg4 is evolutionarily conserved from yeast to mammals.

Atg4 is an essential factor in the Atg8 conjugation system, which is a unique mechanism in autophagy. In this system, Atg4 permits the exposition of the

glycine residue at the C-terminus of Atg8.The C-terminus of processed Atg8 is then adenylated by Atg7, in an ATP-dependent manner, forming an Atg8-Atg7 thioester intermediate. This intermediate enables Atg8 to form a thioester intermediate with Atg3. Finally, Atg8 is transferred to the amino-group of phosphatidylethanolamines (PE), resulting in the Atg8-PE conjugate where the C-terminal carboxyl moiety of Atg8 is covalently attached to the amine group of PE via an amide-bond. Atg8-PE has as mammalian counterpart the LC3-PE. Furthermore, Atg4 cleaves Atg8-PE, making a deconjugation between the C-terminal carboxyl moiety and the amine group of PE. Deconjugation of Atg8-PE by Atg4 has two different roles, notably recycling Atg8 for the next turn of the conjugation reaction, and promoting the elongation step of the isolation membrane. The processing reactions of Atg8 by Atg4 are important for autophagosome formation. For this reason, the inhibition of Atg4 leads to the inhibition of autophagy at the step of autophagosome formation [45].

1.2.9 Atg7

Atg7, together with Atg5, is considered to be an essential molecule for the induction of autophagy.

Atg7 is an E1-like enzyme that activates and forms a thioester bond with Atg8. Successively, Atg8 is transferred to Atg3, which is an E2-like enzyme, and conjugated with phosphatidylethanolamine.

Atg7 is essential for the early elongation and closure of the autophagosomal membrane [46].

Moreover, Atg7 is required for the conjugation of Atg12 to Atg5. The actions of Atg3, as E2-like, and the Atg5–Atg12 complex, as E3-like enzymes, mediates the conjugation of phosphatidylethanolamine to LC3. This event happens together with the translocation of LC3 from the cytosol to the isolation membrane, and this is the reason for which this translocation is considered to be a good marker of autophagy. In the final step, UV radiation resistance associated gene (UVRAG) and the PtdIns3K complex, promote autophagosome–lysosome fusion [47].

1.2.10 ULK1

The ULK1 (unc-51 like autophagy activating kinase 1) complex initiates autophagy. The human ULK1 complex consists of the ULK1 protein kinase itself, the FIP200 (FAK family kinase interacting protein, known as RB1CC1) scaffold, and the HORMA (Hop/Rev7/Mad2) domain-containing proteins ATG13 and ATG101.

Amino acid and energy status are regulating ULK1 via the mTORC1 (mechanistic target of rapamycin-1) and AMPK (AMP-activated protein kinase) kinases. mTORC1 integrates input from growth factors, oxygen levels, amino acid and energy status and promotes protein synthesis and other anabolic processes involved in cell growth and metabolism. When mTORC1 is active causes the inhibition of autophagy by the phosphorylation of both ULK1 and ATG13, causing the reduction of the ULK1 kinase activity.

The demonstration that regulation of ULK1 is a key step in autophagy induction downstream of mTORC1 inhibition, is given by the fact that inhibiting chemically ULK1 prevents rapamycin from initiating autophagy.

AMPK is another regulator of ULK1. It perceives the cellular energy status and is activated when intracellular AMP increases and ATP availability decreases.

By inactivating mTORC1, AMPK indirectly activates the ULK1 complex. AMPK, directly phosphorylating ULK1 in the linker region between the kinase and C-terminal domains, stimulates autophagy. AMPK also phosphorylates ATG13 [48].

In order to transduce cellular signals to downstream events in autophagy, ULK1 phosphorylates Ser14 in BECN1, activating the PI3KC3 complex and promoting autophagy. Moreover, ULK1 interacts with LC3 through the conserved motif LIR (LC3-interacting region), thus allowing the binding of cargo adaptors and core autophagy initiation components [49].

1.2.11 Lysosome

During the intracellular catabolic process, the autophagosome, containing cytoplasmic components, fuses with an organelle, called lysosome, and

exposes cargo to the lysosomal enzymes causing degradation of the content, a process well-conserved from yeast to humans [50].

The lysosome was discovered in 1955 by the Belgian cytochemist Christian de Duve. He named the organelle “lysosome”, based on its lytic function. In fact, the organelle could enclose acidic phosphohydrolase, which is most active at acidic pH.

In the following years, the lysosomes knowledge has increased. Clark observed lysosomes with an electron microscope, founding irregularly shaped bilayer membrane vesicles enveloping amorphous materials, including mitochondria. They were described as ‘irregular density bodies’ and ‘dense bodies’. Presumably, that was the first report of autophagosomes.

In 1962, Ashfold and Porter found that lysosomes membrane enclosed semi-digested mitochondria and endoplasmic reticulum, while Novikoff and colleagues observed an increase in autophagosomes in liver tissue sections from starved rats (peripheral bodies).

In the 1970s, it was found that lysosomes preferentially degrade long-lived proteins

compared with short-lived proteins, be they endogenous or exogenous proteins. Dice and colleagues found that in liver and muscle, the degradation of bigger proteins is faster than that of smaller proteins, and also that the degradation of acidic proteins is faster than that of neutral or basic proteins. Moreover, the degradation of glycoproteins is faster than that of non-glycoproteins. In addition, in rats with diabetes or under starvation, protein degradation is accelerated. All these changes have been confirmed to be due to the activation of non-selective autophagy [31].

The terminal step of autophagy is the autophagic lysosome reformation (ALR). During ALR, reformation tubules are extruded from autolysosomes, and newly lysosomes are generated. Thus, ALR is important for maintaining lysosome homeostasis and ensuring the turnover of autophagolysosomal contents [32].

1.2.12 mTOR

The mechanistic/mammalian target of rapamycin (mTOR) is a serine-threonine kinase that controls several important aspects of mammalian cell function. The activity of mTOR is regulated by intracellular and extracellular factors, and can influence rates of translation, transcription, protein degradation, cell signaling, metabolism and cytoskeleton dynamics.

Interestingly, rapamycin is a natural product which was isolated from *Streptomyces hygroscopicus*, discovered on the island of Rapa Nui in 1972 [51].

In higher eukaryotes, a single gene encoded for mTOR, while its protein product is a component of two distinct complexes, mTOR complex 1 (mTORC1) and 2 (mTORC2), respectively. mTORC1 and mTORC2 are different from each other for their function, structure and their sensitivity to rapamycin. They are sharing some components, mLST8 and DEPTOR, whereas RAPTOR and PRAS40 are present exclusively in mTORC1, while RICTOR, mSIN1, and Protor-1/2 are present only in mTORC2.

One of the main functions of mTORC1 is the protein synthesis regulation, mediated via the phosphorylation of many substrates.

Several members of the AGC family of kinases (i.e. AKT and SGK1) are regulated by mTORC2. It has also a role in the regulation of cytoskeletal organization and has been implicated in the degradation of newly synthesized polypeptides. Moreover, is reported its involvement in the glucose and lipid metabolism through AKT-dependent and independent mechanisms and controls ion transport via SGK1. mTORC2 affects the cytoskeleton and cell migration through protein kinase C alpha (PKCα). In addition, both AKT and SGK negatively regulate FOXO1/3A (forkhead box protein O/O3A), which are transcription factors that regulate metabolism and apoptosis.

mTORC2 is insensitive to short-term rapamycin treatment (24 hours circa), but is downregulated during longer rapamycin exposure *in vivo* [52].

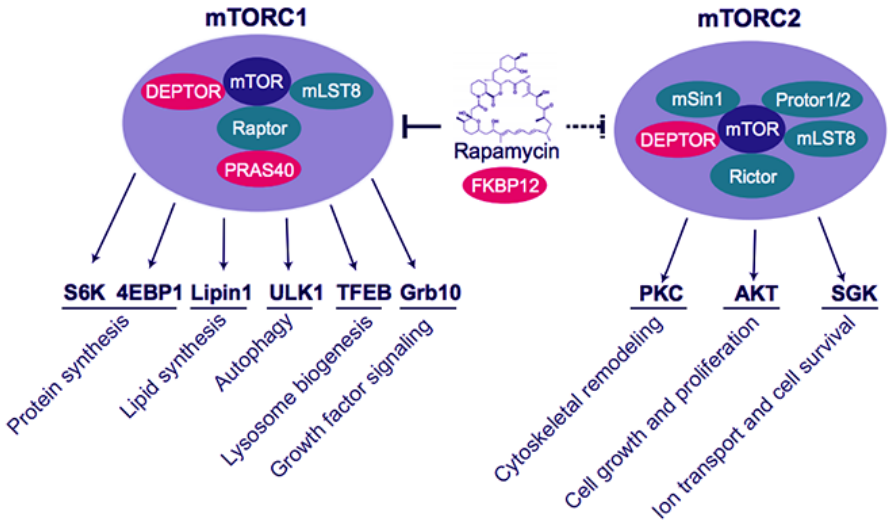

Fig. 1.3 *Components of the mTORC1 and mTORC2 complexes (cite from Meng et al., mTOR signaling in stem and progenitor cells, 2018).*

1.2.13 AMPK

AMPK plays the central role in cell energy metabolism. It is capable to regulate many metabolic processes either by directly acting on metabolically relevant proteins or by indirectly influencing gene expression. In 2011, the Dr. Kun-Liang Guan group found that AMPK and mTOR regulate autophagy by phosphorylating ULK1.

During starvation, AMPK phosphorylates Ser317 and Ser777 activating ULK1 and inducing autophagy. ULK1 is phosphorylated directly in its multiple sites present in the central IDR (intrinsically disordered region) [31]. When the nutrient level is sufficient, the increased mTOR activity induce the phosphorylation of Ser757 to block ULK1 activation, blocking the interaction between ULK1 and AMPK. This study unveiled the mechanism by which AMPK/mTOR regulates autophagy via autophagy-related genes [53].

AMPK is a heterotrimeric complex composed of a catalytic α-subunit and two regulatory subunits (β and γ).

The N-terminus of the AMPKα subunit contains a serine/threonine-protein kinase domain, which is the active center of the AMPK complex.

The AMPKβ subunit contains a flexible, glycine-rich segment with a myristoylation site at the N-terminus, followed by a carbohydrate-binding domain, which is the glycogen-binding domain. Myristoylated AMPKβ has

been reported to cause localization of AMPK to lysosomes upon glucose starvation [54].

The myristoylation is a modification in the lipidation which happens exactly where a myristoyl group is covalently attached to the alpha-amino group of an N-terminal glycine residue. This is given by an amide bond, and is functioning in a variety of signal transduction pathways.

The three alternative γ subunits contain variable N-terminal regions that interact with the β-C-terminal domain (CTD). The N-terminus is followed by four tandem repeats of a motif known as the Cystathionine β-synthase–4 (CBS) repeat, containing binding sites for regulatory nucleotides including AMP, ADP, and ATP. The four CBS repeats in the AMPKγ subunits form a flattened disk shape, and the center contains four potential nucleotide-binding sites (NBS1–4).

The AMPK is characterized by different tissue distribution and cell localizations.

AMPKα1 mainly localizes in the cytoplasm, while AMPKα2 is mostly located in the nucleus. The AMPKγ subunit localizes to muscle fibers, whereas myristoylation of the β subunit enables AMPK to localize to the outer membrane of mitochondria and lysosomes.

The regulation of AMPK is made by LKB1. The level of phosphorylated LKB1 (p-LKBl) is positively correlated with AMPK activity. The key molecular step in the LKB1-mediated activation of AMPK is its phosphorylation at Thr172 within the catalytic α subunit, and this process is facilitated by the binding of AMP to the γ subunit of AMPK.

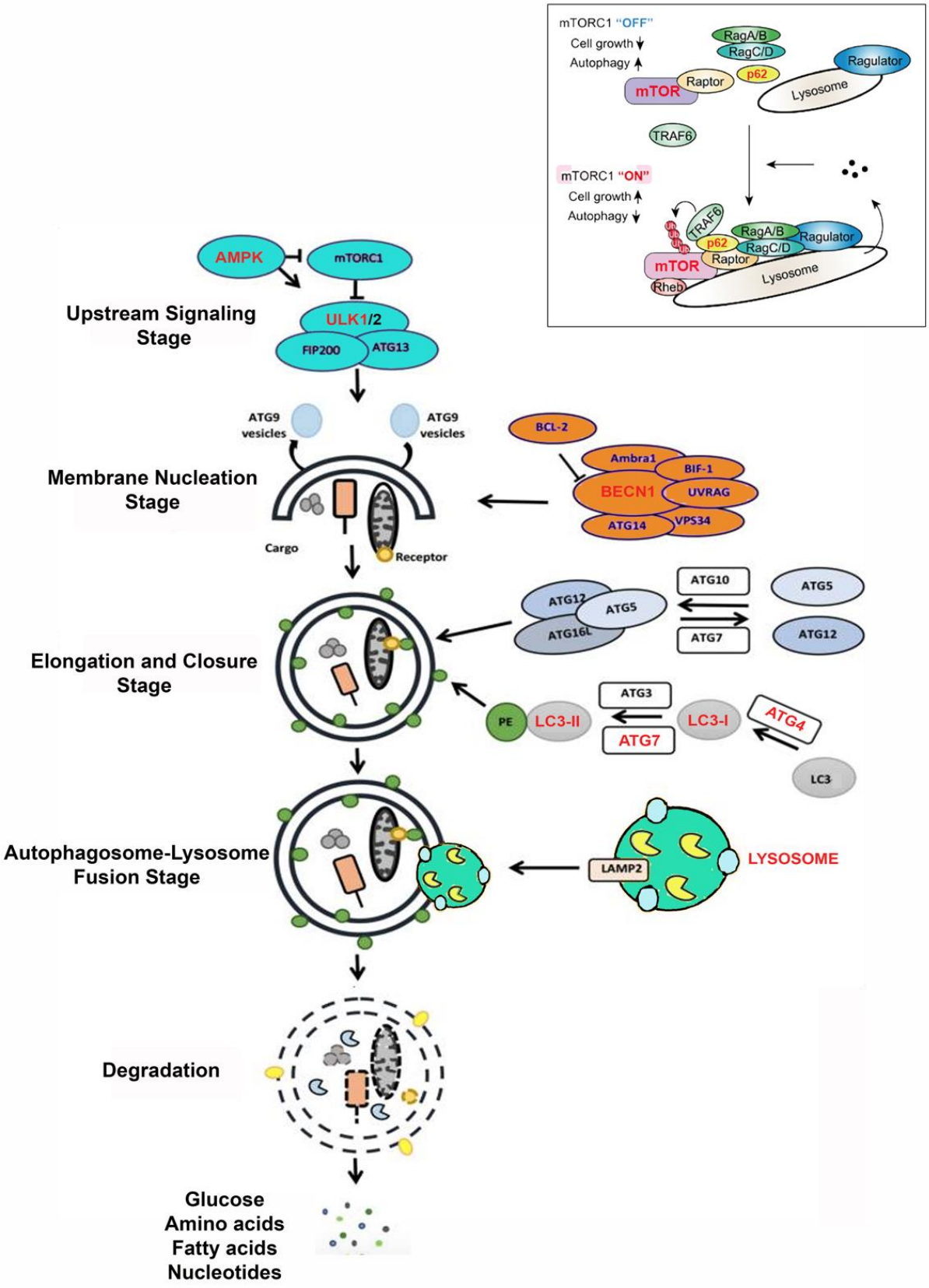

Fig. 1.4 *Stages of the autophagy pathway. The autophagy components highlighted in red are described in this thesis.*

1.2.14 Autophagy in Pompe disease

The autophagy has a critical and central of role in cellular metabolism, and it might be dysregulated in some of the glycogen storage disorders.

Pompe Disease was the first glycogen storage disorder linked to autophagy. When GSD II was first described in the 1930s, there were already inklings about its relationship to autophagy. In fact, the increased glycogen in affected tissues was described as being stored in vacuoles, later determined to be lysosomes.

Successive studies showed an increase in autophagosome number in patients muscle tissue: they were unable to fuse properly with lysosomes, impairing the autolysosome formation [55].

The accumulation of autophagosomes and lysosomes in the cytoplasmic space, and the enlargement and rupture of lysosomes, is the cause of impaired muscle contractility [56]. These findings were observed both in the severe classic IOPD form and during the end stages of LOPD. This autophagic build-up also may reduce the efficacy of ERT, resulting difficult for rhGAA to reach the inside lumen of lysosomes [57].

1.3 Zebrafish (*Danio rerio*)

Zebrafish (*Danio rerio*) is a teleost fish (from Greek: teleios, "complete" + osteon, "bone"), member of the *Cyprinidae* family. The species hailing from Southeast Asia, where lives and proliferate in fresh water reservoir, as rivers, drains, basins, paddy fields and channels.

Zebrafish have been used as research organisms since the 1960s, becoming a popular laboratory model to study genetics, developmental biology, and gene function. They possess a unique combination of features, that make them amenable for many research fields: high fecundity, optical transparent embryos, extra-uterine fecundation, rapid development and easy genetic manipulation.

Zebrafish are a member of the teleost lineage, which had a whole genome duplication event in the late Devonian, after the divergence of the lob finned and ray finned fish [58,59].

The zebrafish genome, even if it has been duplicated 270 million years ago, share a high degree of genetic similarity with humans. At least 71% of human genes have one orthologous zebrafish gene, and 82% of the genes listed in Online Mendelian Inheritance in Man (OMIM) have at least one zebrafish ortholog [60].

The high level of orthology between the zebrafish and human genome, made it become an important research model to understand human disease-related genes [61-63].

The entire amount of data produced by researchers that are using zebrafish, is collected and curated by the Zebrafish Model Organism Database (ZFIN, https://zfin.org), which works as a central repository for zebrafish developmental, genetic, genomic, and phenotypic information [64].

1.3.1 Genetics

The Wellcome Trust Sanger Institute started the zebrafish genome sequencing project in 2001, and the full genome sequence of the Tübingen reference strain is publicly available at the National Center for Biotechnology Information (NCBI)'s Zebrafish Genome Page.

The strategy chosen resembled the clone-by-clone sequencing approach, adopted previously for both the human and mouse genome projects. The Zv9 assembly is a hybrid of high-quality finished clone sequence (83%) and whole-genome shotgun (WGS) sequence (17%), with a total size of 1.412 gigabases. The clone and WGS sequence is tied to a high-resolution, high-density meiotic map called the Sanger AB Tübingen map (SATmap) [60].

The zebrafish reference genome sequence is annotated as part of the Ensembl project, and is maintained by the Genome Reference Consortium. Currently, the most recent is the Genome Reference Consortium Zebrafish Build 11 (GRCz11) version.

Zebrafish possess 26,206 protein-coding genes, more than any previously sequenced vertebrate, presenting a higher number of species-specific genes in their genome than do human, mouse or chicken. Some of this increased gene number is a consequence of the teleost-specific genome duplication [60].

The genome of zebrafish is organized into 25 chromosome pairs, therefore showing 50 chromosomes as diploids, with a remarkable conservation of chromosome numbers, as the majority of teleost. Investigations on karyotype have reported the presence of heteromorphic sex chromosomes. The females (WZ) present a submetacentric Z chromosome and a metacentric W chromosome, while males (ZZ) two submetacentric Z chromosomes [65].

Moreover, zebrafish have peculiar features of chromosomal DNA, such as a unique repeat content, a scarcity of pseudogenes, an enrichment of zebrafish-specific genes and an abundance of type II transposable elements. The abundance of the latter, or the lack of retrotransposable elements, may explain the reason for the low zebrafish pseudogene content [60].

1.3.2 Zebrafish and human diseases

Despite the evolutionary distance between zebrafish and man, the morphogenetic and molecular mechanisms are highly conserved. These

mechanisms, which are present at the embryonic development and genetic programming onset, if altered are the main cause of diseases. Zebrafish have been successfully used to understand the biological activity of genes orthologous to human disease-related genes. This became easier after the investigation of the number of potential disease-related genes, which identified at least one zebrafish orthologue for 3,075 of the 4,023 human genes implicated in genome wide association studies (GWAS) [60]. Furthermore, during the past 15 years, the researchers generated many transgenic zebrafish lines, expressing desired transgenes in either specific subsets of cells or a wide range of tissues and cells, as a powerful tool to study disease related genes.

In terms of anatomy and evolution, the mouse is closely related to human. In fact, there are obvious differences between the zebrafish and mammalian models with regard to physiology and anatomy. About skeletal muscles, for example, slow and fast muscle fibers are not mixed, but topographically separated.

Anyway, several factors may limit the use of mouse as a disease model. For example, it will be challenging to model a congenital disease in a murine model, when the embryonic lethality is caused by secondary defects. Contrarily, zebrafish embryos develop ex utero and their cardiovascular function is not essential during early embryogenesis. Actually, oxygen is sufficiently supplied by bulk diffusion through the skin: developing zebrafish embryo can bypass these secondary defects, and serve as a useful model for investigating the primary cause of a disease at a cellular and molecular level [66].

In addition, is to be remembered that genes essential for muscle development and integrity are highly conserved between mammals and zebrafish (Ensembl, http://www. ensembl.org).

Furthermore, a number of antibodies used in clinical diagnosis cross react with the corresponding zebrafish muscle proteins, thereby providing useful tools for studying human muscle diseases in this vertebrate model.

Again, zebrafish is a powerful tool for the investigation of the autophagy pathway and its role in many diseases [67].

Besides to the ease of genetic manipulation, zebrafish is also useful to pharmacological manipulation, for example to test therapeutic strategies in zebrafish disease models: larvae can be positioned in multiwell plates, and compound requirement is exiguous.
In conclusion, zebrafish offers unquestionable advantages over equivalent murine models, even only because the manifestation of disease phenotypes is typically more rapid than rodents models.

1.3.3 Myogenesis in zebrafish

The formation of muscles occurs after subsequent myogenic waves, regulated by intrinsic and extrinsic signals during mammalian development [68]. This is beginning during the somitogenesis stage, in which the somites originate from the paraxial mesoderm. The dorsal part of an amniotic somite activates the dermomyotome, a transient epithelial structure, which induces the formation of the dermis and the myotome. In zebrafish, which are non-amniotes vertebrates, the initiation of muscle development occurs before the onset of somitogenesis. The first muscle fibers that are formed are the slow twitching fibers, derived from medial adaxial cells [69]. The adaxial originating cells undergo to a myogenic fate and express the myogenic regulator factors (MRFs) myoD and myf5 [70]. After the formation of somite, the adaxial cells migrate laterally from the notochord and elongate on the myotomal surface into superficial slow fibers (SSFs). Successively, they start to express slow myosin heavy chain (MyHC) [68]
After the migration of slow fiber precursors, the fast fibers are specified in the deeper part of the somite and express fast MyHC. At the stage of 24 hpf, segmentation is complete and a functional myotome is formed [68].
Following this primary myogenic wave in zebrafish, secondary slow twitching fibers differentiate in several body locations in a process called secondary myogenesis (48-72 hpf) [71,72]. The mechanism of myotomal growth is very similar to the amniotes. First, the slow muscle fibers number increases, passing from a monolayer to a thicker layer, and initiate to grow towards the dorsal and ventral side of the myotome. Successively, the fusion of muscle fibres is starting, where the mononucleated myoblasts will

become multinucleated myotubes. The myofibre formation process is called myofibrillogenesis.

Due to the somite evolution, boundaries are formed. These will inhibit the elongation of the muscle fibers. The first formed boundary is the initial epithelial somite boundary, which will successively change into a transitional boundary. During this second boundary formation, muscle fibers migrate radially, and focal adhesion molecule appears at the boundary site. In this stage, the chevron-shaped somite becomes visible.

The final boundary evolution part, is the myotome boundary formation. This particular boundary is rich of extracellular, focal adhesion and dystroglycan components [73-75].

The assembly of structural proteins, as actin, alpha-actin, myosin and titin, is necessary to enable the development of highly organized striated muscle. Recently, Samuel R. Keenan and Peter D. Currie published a very interesting review that make a point on discoveries on the zebrafish primary myotome and myofibrillogenesis formation, opening the horizon for further molecular discoveries regarding secondary myogenesis, still under study [76].

1.3.4 Behavioral tests

In order to characterize the muscular phenotype, the behavioral studies are very important.

Zebrafish is a day-active fish, that hides in the dark in response to danger. Males exhibit territoriality, including dancing movements and agonistic behavior. Zebrafish embryos, from 24-26 hours post fertilization, already exhibit simple sensory and locomotor abilities. Some simple behavioral tests concerning locomotion of the embryos have been described in the literature, like rhythmic tail movements, the escape response and the touching assay [77].

The easiest test is based on touching the embryo tail with a plastic needle, in a determined spot, and in evaluating the escape response to the stimulus.

1.3.5 Gene knockdown technologies in zebrafish

Currently, the techniques to perform gene-specific and target-selected mutagenesis in zebrafish are well developed. In addition to the impressive new generation approaches, that take advantage of Zinc fingers nucleases (ZFNs), Transcription activator-like effector nucleases (TALEN) and CRISPR-Cas9, the use of antisense modified oligonucleotides (morpholinos, MOs) technology is still broadly used to produce knockdown zebrafish, in order to study gene function.

Morpholinos (MOs) are synthetic oligonucleotides of 25 bases, which hybridize specifically to complementary sequences of mRNA, disrupting translation initiation or pre-mRNA splicing.

The backbone of MOs is similar to the backbone of DNA or RNA, but with some changes. Specifically, the ribose or deoxyribose sugar molecules that link the bases of the DNA or RNA are replaced by morpholino rings. Anionic phosphates of bases replace non-ionic phosphorodiamidate linkages. Due to this modified backbone, the MO is uncharged, very stable and cannot be degraded by nucleases (www.gene-tools.com).

The translation reduction is never the total, but is still very high, and for this reason is called “knockdown”.

Zebrafish embryos showing a phenotype, as consequence of a MO administration, are called morphants. The MOs are microinjected in the cytoplasm of a 1-cell stage embryo, where will diffuse into the cell. MOs are dissolved in Danieau buffer, and 0,2% Phenol Red is used as an injection tracer. MOs will directly bind to endogenous mRNAs, disrupting the translation initiation. MOs can also be designed against a splice junction, thereby preventing the correct splicing into a mature mRNA [78].

This aberrant splicing includes exon deletion or intron insertion, which might lead to premature stop or a non-functional protein (www.gene-tools.com). Knockdown of gene function is transient and effective until 5 days of development due to dilution of the MOs. MOs exert their effect throughout embryogenesis in a dose-dependent manner.

MO microinjection might cause non-specific side effects. For this reason, control experiments are necessary. Both, a mismatch MO injection, or a

targeted mRNA and MO co-injection, in order to rescue the phenotype, could be considered control experiments.

The efficacy of target protein depletion has to be analyzed by Western blot technique, using a specific antibody direct against the target protein. However, this can only be applied for MOs that disrupt translation. For MOs that result in aberrant spliced mRNA, all outcomes have to be characterized and quantified by RT-PCR [79].

1.4 Acid 3-Bromopyruvic

The Acid 3-Bromopyruvic (3-Bromopyruvic Acid; 3-BrPA) is the organic compound with the formula BrCH2COCO2H. It is the brominated derivative of pyruvic acid, and it presents as a colorless solid. 3-BrPA shows structural similarity to lactic and pyruvic acid. It is a strong alkylating agent.

Besides, 3-BrPA is an inhibitor of hexokinase (HK) a key glycolytic enzyme and has been studied *in vitro* and *in vivo* as an effective anti-tumor drug. 3-BrPA has been shown to be effective in particular in tumors where neoplastic cells preferentially depend on aerobic glycolysis to produce adenosine triphosphate (ATP) for growth and proliferation [80-83]. This phenotype, referred to as ‘aerobic glycolysis’, was first observed by Warburg in 1924. The anti-cancer property of 3-BrPA is due to its ability to inhibit glycolysis, by abolishing cell ATP production and consequently impeding transformation of glucose into glucose-6-phosphate by hexokinase [84], and to trigger activation of the autophagic process [85].

In mammals, separate genes code for different hexokinase isoforms: HKI, HKII, HKIII, and HKIV. HKII is expressed at relatively high level only in skeletal muscle, adipose tissue, and heart.

HKII is responsible for the conversion of glucose to glucose-6-phosphate in the first step of glycolysis without being regulated by negative feedback (product inhibition) as are the other hexokinase isoforms [86]. Furthermore, HKII it is reported to be one of the 3-BrPA major targets [87,88].

Since 3-BrPA presents structural/chemical similarities to lactate, it is likely that it is transported across the plasma membrane of cells by the proton-linked monocarboxylate transporter (MCTs) [89]. Nine MCT-related

sequences have so far been identified in mammals, each having a different tissue distribution. In particular, MCT1 is ubiquitously expressed, but is especially prominent in heart and red muscle, while MCT4 is most evident in white muscle and other cells with a high glycolytic rate, such as tumor cells and white blood cells, suggesting it is expressed where lactic acid efflux predominates [90].

It has been reported that the alkylating agent 3-BrPA has slight toxicity with production of ROS for normal cells and does not completely abolish respiration and ATP synthesis [91]. In contrast, in cancer cells where MCTs are over expressed and glycolytic metabolism is exacerbated, 3-BrPA can accomplish its anticancer and deleterious effect to the cells [92].

The fact that the zebrafish hexokinases isoforms and their proton-linked monocarboxylate transporters are very similar and comparable to the mammalian ones [93,94], makes zebrafish a reliable model for studying 3-BrPA effects.

1.5 Aims of the study

The aim of this study is the generation and characterization of a zebrafish PD model, obtained by knocking down the GAA gene, and the evaluation of possible therapeutic effects of 3-BrPA on glycogen accumulation and on autophagy

We generated and characterized the zebrafish PD knock-down model obtained using two different morpholinos, one designed against the ATG translational start codon and one against a splice site of the zebrafish gaa transcript, to create a model in which the glycogen will be massively accumulated in the muscle. We will then assess formation, storage and metabolism of glycogen in zebrafish embryos.

We estimated the modulation of autophagy, pre- and post- 3-BrPA administration, by Western blot, immunocytochemistry and qRT-PCR.

Furthermore, we injected the endogenous gaa mRNA into the zebrafish PD embryos, to mimic the effects of Enzyme Replacement Therapy. Successively we treated the rescued morphants with 3-BrPA, in order to evaluate the treatment action on rescue.

In order to demonstrate the effectiveness of the treatment, we carried out analysis of muscle morphology at optical and ultrastructural level, performed statistical, immunochemical, immunohistochemical analysis, and optical microscopy.

We proposed to use 3-BrPA, an inhibitor of a key glycolytic enzyme (HKII), as a method to reduce glucose uptake into the cell and to modulate autophagy in the muscular system. Our study provided an in-vivo proof-of-principle that this compound potentially represents a feasible treatment that can improve muscle function, quality of life and life expectancy in PD patients who have shown mild or no improvement with ERT.

We strongly believe that the relevance of this study lies on the possibility to find a novel adjunct therapy for this pathology.

Moreover, we are confident that the zebrafish PD model will result in a suitable tool for different scientific fields, supporting investigation improvements in this pathology under many perspectives, including helping to shed light on impact of PD in heart and central nervous system.

We also believe that the use of 3-BrPA, if efficacious in PD, could be extended to other disorders including Lafora disease which is characterized by glycogen accumulation in the brain and autophagy impairment.

2

Glycogen storage in a zebrafish Pompe disease model is reduced by 3-BrPA treatment.

Cinzia Bragato, Silvia Carra, Flavia Blasevich, Franco Salerno, Alessia Brix, Andrea Bassi, Monica Beltrame, Franco Cotelli, Lorenzo Maggi, Renato Mantegazza, Marina Mora.

https://doi.org/10.1016/j.bbadis.2020.165662

Accepted 2 January 2020.

2.1 Abstract

Pompe disease (PD) is an autosomal recessive muscular disorder caused by deficiency of the glycogen hydrolytic enzyme acid α-glucosidase (GAA). The enzyme replacement therapy, currently the only available therapy for PD patients, is efficacious in improving cardiomyopathy in the infantile form, but not equally effective in the late onset cases with involvement of skeletal muscle. Correction of the skeletal muscle phenotype has indeed been challenging, probably due to concomitant dysfunctional autophagy. The increasing attention to the pathogenic mechanisms of PD and the search of new therapeutic strategies prompted us to generate and characterize a novel transient PD model, using zebrafish. Our model presented increased glycogen content, markedly altered motor behavior and increased lysosome content, in addition to altered expression of the autophagy-related transcripts and proteins Beclin1, p62 and Lc3b. Furthermore, the model was used to assess the beneficial effects of 3-bromopyruvic acid (3-BrPA). Treatment with 3-BrPA induced amelioration of the model phenotypes

regarding glycogen storage, motility behavior and autophagy-related transcripts and proteins. Our zebrafish PD model recapitulates most of the defects observed in human patients, proving to be a powerful translational model. Moreover, 3-BrPA unveiled to be a promising compound for treatment of conditions with glycogen accumulation. Keywords: Pompe disease, acid α-glucosidase, zebrafish, glycogen, 3-Bromopyruvic acid (3-BrPA).

2.2 Abbreviations

3-Bromopyruvic acid (3-BrPA),
Hexokinase (HK),
2-(N-(7-nitrobenz-2-oxa1,3-diazol-4-yl)-amino)-2-deoxyglucose (2-NBDG),
morpholino (MO),
standard control morpholino (STD-Ctrl),
hours post fertilization (hpf),
days post fertilization (dpf).

2.3 Introduction

Pompe disease (PD), also called glycogenosis type II, is an autosomal recessive metabolic disorder due to a defect in the lysosomal enzyme acid α-glucosidase (GAA), or acid maltase, necessary for glycogen degradation. The defect results in generalized excessive glycogen accumulation in tissues, involving in particular skeletal and cardiac muscle.

The spectrum of disease severity encompasses a broad continuum of phenotypes ranging from the most severe “classic” form, characterized by child onset, severe cardiomyopathy, rapidly progressive course and fatal outcome before two years of age, to the “intermediate” infantile form with milder phenotype, to the juvenile and adult forms with prevalent involvement of skeletal muscle [12]. The almost total deficiency of the enzyme results in the severe infantile form, while partial deficiency is responsible for the intermediate and mild forms [4,95].

The enzyme replacement therapy (ERT), the only medication available since 2006, has represented a major step in the treatment of patients with Pompe disease and, although gene therapy is in clinical trial, currently it remains the only FDA-approved therapy. ERT has shown to be effective in improving cardiomyopathy in the infantile severe Pompe disease form; however, despite clinical benefits for most patients [9-11,96,97] the late onset cases do not all respond equally well to treatment, and a number of reports suggests that correction of the skeletal muscle phenotype is particularly challenging, probably due to concomitant altered autophagy [17-20]. However, it remains unclear how autophagy, a key molecular mechanism that maintains cellular homeostasis and ensures
correct macromolecule turnover in the cell [98-100], is responsible for GAA failure to restore muscle function, since it is yet unknown if an excessive acceleration or reduction of the process is present in Pompe disease.

The possible role of altered autophagy has stimulated both reassessment of the pathogenic mechanisms and investigation of novel therapeutic approaches in Pompe disease, including searching for adjunctive and alternative therapies addressing both glycogen accumulation and autophagy [101-106].

Among the small molecules to be explored for interfering with glycogen accumulation, we have developed an interest on 3-bromopyruvate (3-BrPA), an inhibitor of hexokinase (HK), which is a key glycolytic enzyme. In vitro and in vivo studies have reported that 3-BrPA is an anti-tumor drug effective in those tumor phenotypes in which cancer cells preferentially depend on glycolysis to produce adenosine triphosphate (ATP) for growth and proliferation [80-83]. This phenotype, referred to as “aerobic glycolysis", was first observed by Warburg in 1924. The anti-cancer property of 3-BrPA is due to its ability to inhibit glycolysis, by abolishing cell ATP production and, consequently, preventing the hexokinase transformation of glucose into glucose-6-phosphate [84], and to trigger activation of the autophagic process [85].

In mammals, separate genes code for different hexokinase isoforms: HKI, HKII, HKIII, and HKIV. HKII is expressed at relatively high levels only in skeletal muscle, adipose tissue, and heart. HKII is responsible for the conversion of glucose to glucose-6-phosphate in the first step of glycolysis without being regulated by negative feedback (product inhibition) as are the other hexokinase isoforms [86]. Furthermore, HKII is reported to be one of 3-BrPA’s major targets [87,88] among all the other hexokinase isoforms.

3-BrPA, having structural similarity with lactate, is likely to be transported across the plasma membrane of cells by the proton-linked monocarboxylate transporter (MCTs) [89]. Of the 9 known MCT-related sequences in mammals, MCT1 is ubiquitously expressed, but is especially prominent in heart and red muscle [90].

At present, the best characterized animal model of PD is the GAA-knockout murine model which lacks *Gaa* mRNA transcription and displays a virtually complete acid α-glucosidase deficiency [107]. Such a model does not recapitulate the genetics of patients affected by late onset Pompe disease, in whom hypomorphic GAA mutations are present [108]. In the present study, we generated a novel transient PD model, taking advantage of zebrafish, to better recapitulate the pathophysiology of these PD patients.

Zebrafish, as reported in the literature in the past years, is a suitable model to study autophagy [109,110]. Moreover, zebrafish hexokinases isoforms and their proton-linked monocarboxylate transporters are very similar and

comparable to the mammalian ones [94,111], making zebrafish a reliable model for studying 3-BrPA effects.

In the present study, we characterized the PD zebrafish transient model using two different morpholinos (a translation-blocking morpholino, against the start codon ATG and a spliceblocking morpholino, against a specific portion between intron 9 and exon 10 of the zebrafish gaa gene). We investigated the effects of rescuing the resulting phenotypes of the latter by injecting an *in vitro* transcribed *gaa* RNA. In gaa morphants we assessed skeletal muscle condition at optical and electron microscopy level, determined glycogen accumulation, and evaluated motor behavior by touch evoked motility test. Finally, we assessed possible beneficial effects of 3-BrPA treatment on glycogen storage, on autophagy related transcripts and proteins and on motility behavior.

2.4 Materials and Methods

2.4.1 Animal care

Fish were raised and maintained according to good animal practice principles as defined by the Italian animal welfare regulations. All experiments were performed on embryos and larvae within 5 days post fertilization (dpf), thus not subject to animal experimentation rules according to European and Italian directives.

2.4.2 RNA extraction and reverse transcription

Total RNA was extracted from zebrafish embryos at different stages, from 1 cell stage to 5 dpf, using TRI Reagent (MRC, Cincinnati, OH, USA). First-strand cDNA synthesis reaction from total RNA was catalyzed by Transcriptor First Strand cDNA Synthesis Kit (Roche Diagnostic, Penzberg, Germany). cDNA was amplified with specific primers using Phusion High-Fidelity polymerase (Finnzymes, Thermo Fisher Scientific, Waltham, MA, USA). The PCR products were purified using Illustra ExoProStar (GE Healthcare, Life Sciences, WI, USA) and sequenced directly with BigDye Terminator v1.1 Cycle Sequencing Kit (Applied Biosystems, Life Technologies, Carlsbad, CA, USA). Sequences were analyzed on an ABI Prism 3100 Genetic Analyzer (Applied Biosystems, Life Technologies, Carlsbad, CA, USA). The primers used to clone the cDNA in the vector were: gaa: 5′-ACATCACAGGAAAATGGCGG -3′ (Forward) and 5′-TCCCGTGAACTTGTAACAGC -3′ (Reverse). Primers used to visualize I9E10gaa-MO in-frame intron retention were: 5’-CTTTACTTTCGACCCGCAGC -3’(Forward) and 5’-AACGGCCGAGTTTTCTTCAC -3’ (Reverse).

2.4.3 Morpholino injections

Zebrafish gaa was knocked down with two different antisense morpholinos: one, called ATG*gaa*-MO, directed against the translation start site of the gaa transcript, 5′-CTTCATGTATTAAACACAGGGCTGT-3′, and one, called I9E10gaa-MO, targeting the splice site between intron 9 and exon 10, close to the region encoding the catalytic site of the Gaa protein, 5′-tgtgattttcttgtttacagGACAT-3′. The latter, in particular, causes retention of intron 10, resulting in insertion of 14 aberrant amino acids and in premature stop codon.

Both morpholinos were designed and purchased, along with a standard control morpholinos (STD-Ctrl), from Gene Tools (Gene Tools, Philomath, OR, USA). Fertilized eggs, collected after timed mating of adult zebrafish, were injected at the 1-2 cell stage using an Eppendorf transferman nk2 micromanipulator (Eppendorf AG, Hamburg, Germany). Embryos were injected with either ATG*gaa*-MO (0.8 pmol/embryo), or I9E10gaa-MO (1 pmol/embryo), or STD-Ctrl (to verify absence of morpholino-mediated toxicity), diluted in Danieau solution in a volume of 4 nl [85]. To monitor the injection either rhodamine dextran (Molecular Probes, Life Technologies, Carlsbad, CA, USA) or phenol red (Sigma Aldrich, Saint Louis, MO, USA) were co-injected as tracers and observed under a Leica MZ FLIII microscope (Leica Microsystems GmbH, Wetzlar, Germany).

For rescue experiments, embryos were injected (4 nl total volume) with I9E10gaa-MO plus gaa mRNA (10pg). After injection embryos were allowed to develop in fish water at 28 °C up to the stage of interest.

Phenotypic assessment was conducted by visual assessment using a stereomicroscope Leica MZ FLIII. Embryo phenotypes were subdivided based on the morphological features described in Kimmel et al., 1995 [86]. Deformities included abnormally curled tails, shortened body length, abnormal somite structure, etcetera.

2.4.4 Western Blot

Dechorionated embryos (minimum 10 per experiment) were boiled for 10 min at 95ºC. Twenty µg of protein samples were electrophoresed on 10%

SDS-PAGE and transferred to nitrocellulose membranes (Bio-Rad Laboratories, Hercules, CA, USA) following standard procedures. The amount of loading proteins was previously determined with serial dilutions (10, 20, 50 µg) in order to have bands of adequate intensity to be detected within the linear range. α-Tubulin, used as loading control, was also diluted in the linear range. The membranes were blocked with 5% nonfat dry milk in TBS, pH 7.5, containing 0.1% Tween 20 (TBST) for 1 h at room temperature, incubated with antibodies reported in table 2.1.

Primary antibodies	**Dilution**		**Company**	**Cat. numb.**	**Lot**
LC3B (NB100-2220)	1:500	polyclonal	Novus Biologicals Europe, Abingdon, UK	NB100-2220	Lot:EC
GAA	1:100	polyclonal	Sigma Aldrich, St. Louis, Missouri, USA	SAB2100872	Lot: QC14285
p62	1:500	polyclonal	PROGEN Biotechnik GmbH, Heidelberg, Germany	GP62-c	Lot:709151
mTOR	1:500	polyclonal	Santa Cruz Biotecnology, Santa Cruz, CA, USA	sc-8319	N/A*
p-mTOR	1:200	monoclonal	Santa Cruz Biotecnology, Santa Cruz, CA, USA	sc-293133	N/A*
AMPk	1:500	polyclonal	Santa Cruz Biotecnology, Santa Cruz, CA, USA	sc-25792	N/A*
pAMPk	1:200	polyclonal	Santa Cruz Biotecnology, Santa Cruz, CA, USA	sc-33524	N/A*
BECLIN1	1:500	polyclonal	Thermo Fisher, MA, USA	PA1-46454	Lot: #SC2360229A
αTubulin	1:1000	monoclonal	Sigma Aldrich, St. Louis, Missouri, USA	T7451	Lot:051M4770
LAMP2 (H4B4)	1:500	monoclonal	DSHB, Iowa, USA	H4B4	N/A

Secondary antibodies	**Dilution**		**Company**	**Cat. numb.**	**Lot**
Amersham ECL Goat anti-Rabbit IgG HRP	1:1000	polyclonal	GE Healtcare Lifescience, Chicago, IL, USA	NA9340V	Lot:16955624
Amersham ECL Goat anti-Mouse IgG HRP	1:1000	monoclonal	GE Healtcare Lifescience, Chicago, IL, USA	NA931V	Lot:16982037
Biotin-SP-conjugated AffiniPure Donkey Anti-Guinea Pig IgG (H+L)	1:1000	polyclonal	Jackson ImmunoResearch, Cambridgeshire, UK	706-065-148	Lot:106654

***Table 2.1** List of primary and secondary antibodies used*

** kind gift from Dr. Giuseppina Caretti's Laboratory, Università degli studi di Milano;*

+ Note that, except for the anti-LC3B antibody, validated in zebrafish (see i.e. Ran et al., 2017), all other antibodies had not been reported in the literature as cross-reacting with Danio rerio proteins. The choice of the right antibody was based on the epitope being at least 40% similar to the zebrafish one.

2.4.5 Yolk removal

For sedation Dechorionated embryos were placed, using a plastic pipette, in an Eppendorf tube (1.5 ml) on ice, for sedation. The embryos were then placed at room temperature (RT), as much fluid (fish water/egg water) as possible was removed from the tube, and deyolking buffer (1/2 Ginzburg fish Ringer solution) was added (*). The yolks were gently removed with a 200 µl pipette tip. The embryos were let floating down to the bottom of the tube, and as much deyolking fluid as possible was removed, 2 rinses with ice cold Ringer's solution followed with liquid removal each time.

(*) Deyolking buffer:

To obtain 400 ml of deyolking buffer, 0.04 g of NaHCO3 were added to a solution composed of 1.3 g NaCl, 0.05 g KCl, 0.06 g CaCl2 or 0.08 g CaCl2 2H2O in 350 ml milliQ water, and adjusted to a final volume of 400 ml with further milliQ water. The solution was filtered and stored at RT.

2.4.6 Glycogen Assay

The glycogen amount was determined in dechorionated zebrafish embryos (minimum 10 per experiment), after yolk removal, by the Glycogen Assay kit II (Abcam, Cambridge, England) according to the manufacturer's instructions.

2.4.7 Embryo morphological characterization

Zebrafish at 4 dpf were fixed 2 h in 2.5% glutaraldehyde-sodium phosphate buffer, pH 7.4; left in buffer overnight at 4 °C; post-fixed 1 h in 2% phosphate-buffered OsO4, dehydrated in graded ethanol, and embedded in epoxy resins (Electron Microscopy Sciences, Hatfield, Pennsylvania). Semi-

thin sections (1 µm thick) were examined by light microscopy after toluidine blue staining. Ultrathin sections of zebrafish tails were collected onto grids, stained with uranyl-less (Electron Microscopy Sciences) and Reinold's solution, and examined with a FEI Tecnai G2 Spirit electron microscope (FEI Hillsboro, Oregon, United States).

2.4.8 Periodic acid–Schiff (PAS) staining

Resin was removed with sodium methoxide (3') from semi-thin sections of 4 dpf zebrafish, followed by methanol (5') and ethanol (5'). For staining, sections were placed in: Carnoy fixative (15'); 2% periodic acid (15'); and Schiff reactive (1 hour in the dark); then they were dehydrated and mounted.

2.4.9 LysoTracker Red dye staining

LysoTracker Red (Thermo Fisher Scientific) was added to embryos at 24 hours post fertilization (hpf) in 48-well plates, at a final concentration of 10 µM. The embryos were incubated at 28.5°C for 45 minutes. Then, the water was removed and the embryos were rinsed three times with approximately 1 ml fresh fish water immediately before fluorescence microscopy imaging, as described [114].

2.4.10 Glycogen visualization with 2-NBDG

2-(N-(7-nitrobenz-2-oxa1,3-diazol-4-yl)-amino)-2-deoxyglucose (2-NBDG) was used to verify if glycogen could be visualized in vivo. This is a fluorescent synthetic glucose analog, hypothetically suitable to be incorporated within the multi-branched polysaccharide glycogen chain rendering it fluorescent. Two hundred pg/embryo of 2-NBDG were injected into wild type embryos at 1 cell stage. Embryos were examined under an epifluorescence microscope at somitogenesis stage and at 24 hpf, and fluorescent glycogen accumulation could be detected in the somites and in the tail (Fig. 2.1). The limitation of this experiment is that 2-NBDG fluorescent signal is visible for about 24 hours, therefore only in embryos

until 1 dpf. A different approach is thus required to detect glycogen in later developmental stages.

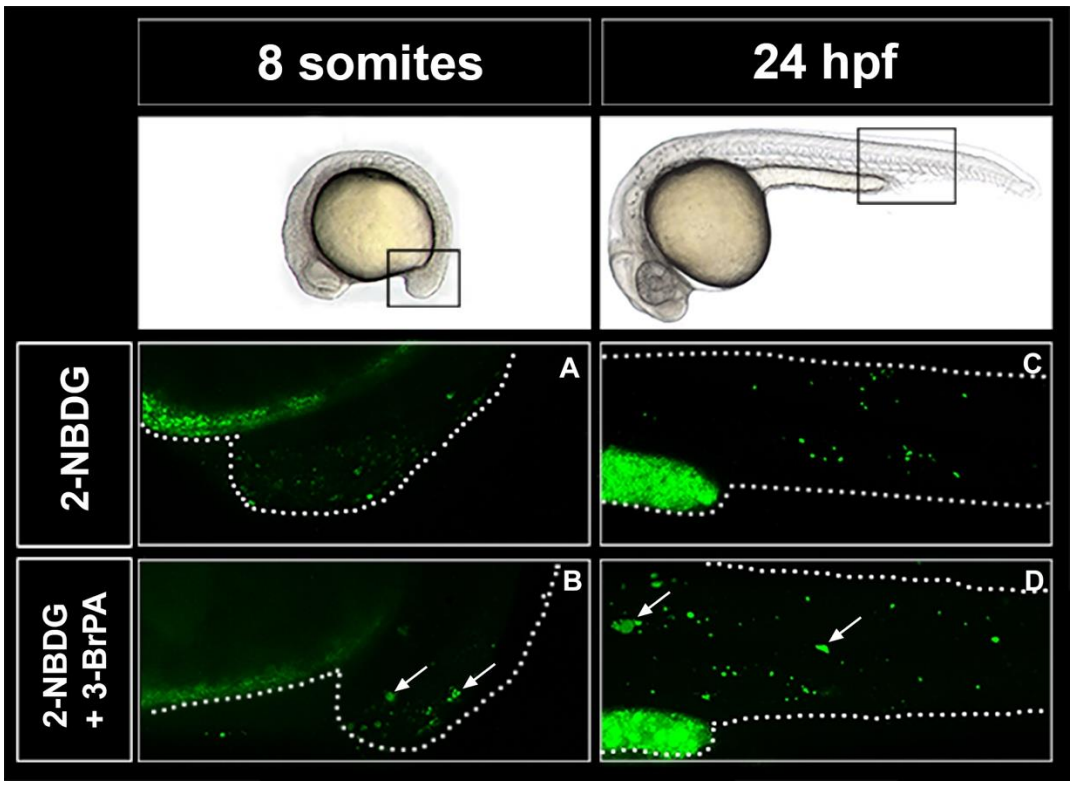

***Fig. 2.1* Wild type zebrafish embryos injected at 1 cell stage with 2-NBDG.** *(A-D) 2-NBDG, a fluorescent 2-deoxyglucose analog, is used to monitor glucose incorporation into glycogen in embryo muscles. Embryos were analyzed under a confocal microscope (Leica Microscopy System SP8). (A, C) Untreated STD-Ctrl embryos at the stage of somitogenesis (8 somites) and at 24 hpf. The images show the glycogen in embryos muscles visualized as green dots. (B, D) Embryos exposed to 3-BrPA treatments at the stage of 60% epiboly stage, and analyzed after treatment at 8 somite stage, when muscle starts to form, and at 24 hpf, when embryos start to present spontaneous movements and need energy for hatching. Note that although fluorescent dots seem larger in total the 3-BrPA treatment does not increase glycogen, but increases the size of autophagolysosomes Scale bar = 200 µm.*

2.4.11 Quantification

To quantify the LysoTracker dye, tricaine treated embryos were observed under an epifluorescence microscope and pictures of the entire tail, starting from one somite before the end of the yolk, were taken at 10X. The red signal area (expressed as arbitrary units) was calculated by means of Fiji software (https://imagej.net/Fiji) on images taken at same exposure conditions [88]. Using the software, a threshold was applied to the pictures

to obtain red and black images with regions positive for LysoTracker in red and negative in black. The area positive for LysoTracker was calculated as a percentage of the entire image, and the mean percentage area was then obtained. The same procedure as before was used to quantify the 2-NBDG green signal.

The quantitation of the western blot bands was performed on membranes from three different experiments using Fiji software. To perform the analysis, for each protein and loading control, a region of interest (ROI) was defined and saved. The same ROI was applied to the other two membranes images, in order to take measurements in the same way for the bands and their background. The ratios between protein band of interest and loading control band, expressed as arbitrary units, were then exported into an excel file and analyzed using Graph-pad Prism software.

2.4.12 qRT-PCR

Transcripts of wild-type gaa and of genes related to autophagy were evaluated by qRTPCR using primers reported in Table 1. PowerUp SYBR Green Mastermix (Thermofisher) and ABI Prism 7000 (Applied Biosystem) PCR systems were used for quantification. ΔΔCt method was used to calculate the relative copies of mRNAs of the gene of interest, normalized to the reference gene mRNA (Table 2.1).

atg4b-Forward	5'-ACACCACTCAGCCAGCAG-3'
atg4b-Reverse	5'-AAGCCAGCAGCAATAGAAGG-3'
beclin1-Forward	5'-GCCATTGTATTGTTCAGGTG-3'
beclin1-Reverse	5'-CAGAAGCCAGTGTCATCC-3'
atg7-Forward	5'-AGAGTCCAGTCCGATGTC-3'
atg7-Reverse	5'-GAAGTAACAGCCGAGACG-3'
p62-Forward	5'-TTTGGCTCTTGTGAAGGATGAC-3'
p62-Reverse	5'-GAGGGCTAAAGTGAGGTGTAGTGA-3'
mtor-Forward	5'-ATACGCATCCAGTCCATTG -3'
mtor-Reverse	5'-TCATTAGCCAGTAGAGTGTTC-3'
lc3b-Forward	5'-CCTCCAACTCAACTCCAACC-3'
lc3b-Reverse	5'-GCCGTCTTCGTCTCTTTCC-3'
Housekeeping gene:	
Ef1a-Forward	5'-CTGTACCTGTGGGTCGTGTGGAGACTG-3'
Ef1a-Reverse	5'-CAGCCTTCTGTGCAGACTTTGTGAC-3'

Table 2.2 ***Primers used for qRT-PCR analyses****. Transcripts of genes related to autophagy were evaluated by qRT-PCR using primers reported in table 1, normalized to the reference gene mRNA (housekeeping gene).*

2.4.13 *gaa* mRNA injection

The cDNA of full-length zebrafish gaa was amplified by RT-PCR using total RNA extracted from whole zebrafish embryos. The primer sequences used were 5′-GCAGGATCCCATCGATGGACATCACAGGAAAATGGCGG-3′ (sense primer plus ClaI sequence) and 5′-GTTCTAGAGGCTCGAGCCTCCCGTGAACTTGTAACAGC-3′ (antisense primer plus XhoI sequence) for zebrafish gaa cDNA. The amplified fragments were inserted into pcGlobin2 vector [89]. After digestion of pcGlobin2 vector with appropriate restriction enzymes (ClaI and XbaI, New England biolabs, Ipswich, MA; and XhoI; Promega Corporation, Madison, WI, USA), the amplified cDNA of gaa was cloned into pcGlobin2 vector to obtain the pcGlobin2-gaa construct. Plasmids were linearized with XbaI

enzyme (New England Biolabs, Ipswich, MA, USA) and transcribed using the T7 mMessage Machine kit (Ambion, Life Technologies, Carlsbad, CA, USA). Fertilized eggs were injected at the one to two cell stage with zebrafish gaa mRNA (10 pg), in a 4 nl volume, using a microinjector (Leica).

2.4.14 3-BrPA treatment

Different concentrations of 3-BrPA, starting from 20 μM to 2 mM, diluted in 20 ml of fish water, were tested, based on published data [117], to evaluate the dose-dependent mortality range (Fig. 2.2). A concentration of 100 μM was chosen to treat the embryos at 60% epiboly stage. Since the 3-BrPA molecule dimension is such that it can cross the chorion barrier, the treatment was administered to embryos with chorion.

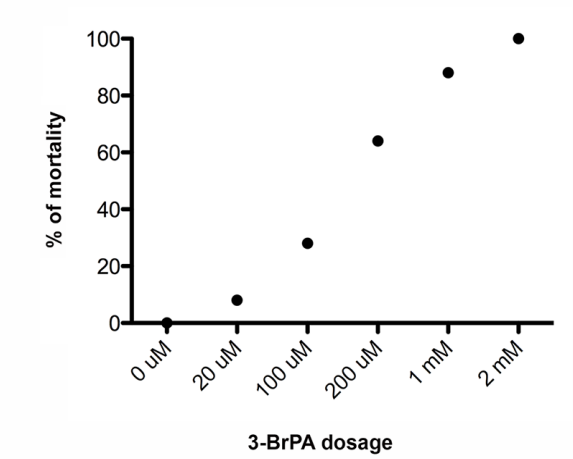

***Fig. 2.2* Evaluation of 3-BrPA dose-dependent mortality range**. *Mortality range increases at increasing concentrations of 3-BrPA, from 20 μM to 2 mM. The concentration of 100 μM was chosen to treat the embryos at 60% epiboly stage.*

2.4.15 Screening for embryonic motility

Larvae were subjected to a tactile stimulus at 3 dpf: using a needle, a gentle stimulus was applied to the tail of the zebrafish larvae and their reaction observed (touch-evoked motility test) [77]. Upon application of the tactile stimulus wild type larvae at this stage of development normally swim away from the source of the stimulus, while embryos injected with morpholino oligonucleotides to knock down genes related to motility show variably reduced motility.

2.4.16 Data Analysis

In all knock down experiments, ATG*gaa*- and I9E10*gaa*-MO-injected embryos were compared to embryos at the same developmental stage, injected with the same amount of a control standard morpholino.

Results were expressed as means ± standard deviation. Differences between groups of morphants in basal conditions (ATG*gaa*-MO or I9E10*gaa*-MO vs STD-Ctrl, 3-BrPA-treated or non-treated) and differences between groups in rescue experiments (I9E10gaa-MO, treated and non-treated, and STD-Ctrl) were assessed by the two-tailed Student T test. P values were considered significant: *$p \leq 0.05$, **$p \leq 0.01$; ***$p \leq 0.001$. For graphs, Graphpad Prism software was used; for figures, Adobe Photoshop was used.

2.5 Results

2.5.1 Characterization of the model

2.5.1.1 Zebrafish *gaa* gene

The *gaa* zebrafish transcript (variant X1) corresponding to NCBI XM_001921922.5 was identified. This is the only full length coding sequence present in zebrafish, located on chromosome 3, and reported as the orthologous of the human gene acid alpha glucosidase (GAA). The identity between the human GAA and the zebrafish Gaa protein is 58% (from Genomicus, www.genomicus.biologie.ens.fr/genomicus/cgi-bin/search.pl). This good similarity is due to the conservation of all the functional domains (Trefoil domain, GH31_N Domain, GH31_MGAM_SI_GAA Domain and Glyco_Hydro_31 Domain) of the protein. The characterization of gaa expression, performed by qRT-PCR, showed that the gaa transcript is present from the first stages of development up to 5 days post fertilization (Fig. 2.3).

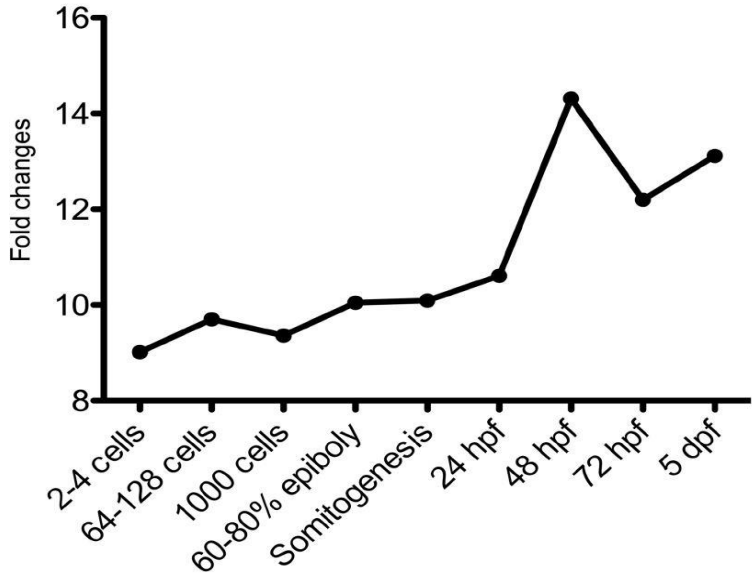

***Fig. 2.3* Expression of the gaa transcript during development in zebrafish**. *qRT-PCR shows the presence of gaa transcript in zebrafish from early developmental stages to day 5.*

2.5.1.2 *gaa* knocked-down embryos displayed phenotypic defects and increased glycogen content

Both gaa morpholinos were tested at a range of concentrations (from 0.5 pmol/embryo to 1.5 pmol/embryo) and dose-dependent phenotypic classes were observed. Based on the observed phenotypic classes, in order to obtain embryos with glycogen accumulation in skeletal muscle, but with an overall conserved somite structure, ATG*gaa*-MO was injected at a concentration of 0.8 pmol/embryo and I9E10gaa-MO at a concentration of 1 pmol/embryo. Since I9E10gaa-MO injected embryos showed a slight growth delay at early stages of development, the phenotypes were examined at 3 dpf.

ATG*gaa*-MO injection resulted in reduced Gaa protein amount, as evaluated by western blot, (Fig. 2.4A), and injection of I9E10*gaa*-MO causing an out-of-frame insertion due to activation of a cryptic splice site (https://www.genetools.com/choosing_the_optimal_target#blockingnuclear processing), resulted in a higher aberrant transcript band, as evaluated by RT-PCR, and in lack of the aberrant protein band by western blot (Fig. 2.4B).

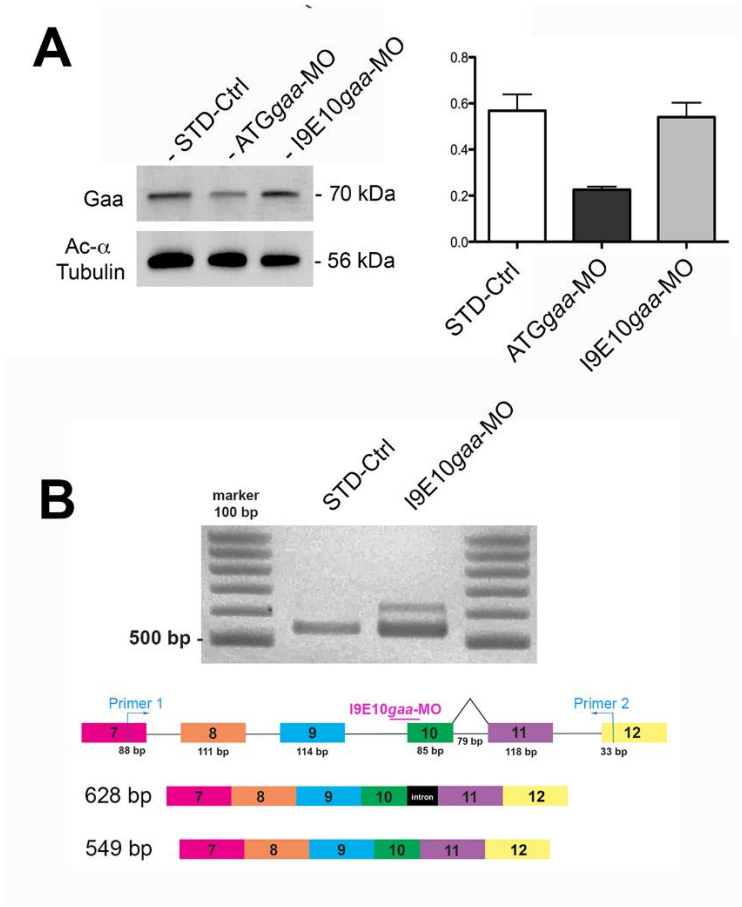

***Fig. 2.4* Morpholinos effects validation.** *(A) Western blot showing reduced Gaa band intensity in the ATGgaa morphants, and graph showing quantitation. (B) Top: Zebrafish gaa transcript fragment of STD-Ctrl and I9E10gaa morphants. I9E10gaa-MO induces insertion of intron 10, corresponding to a 628 bp band, higher than the 549 bp normal band. Bottom: schematic representation of the bands shown in the gel.*

At the chosen concentrations, of the embryos injected with ATG*gaa*-MO, 285 (69 % of total) pertained to the C1 class with normal-appearing morphology and completely formed somites, 95 (23% of total) pertained to the C2 class with partially disrupted somites, and 36 (8% of total) pertained to the C3 class (Fig. 2.5) with unformed or totally disrupted somites;

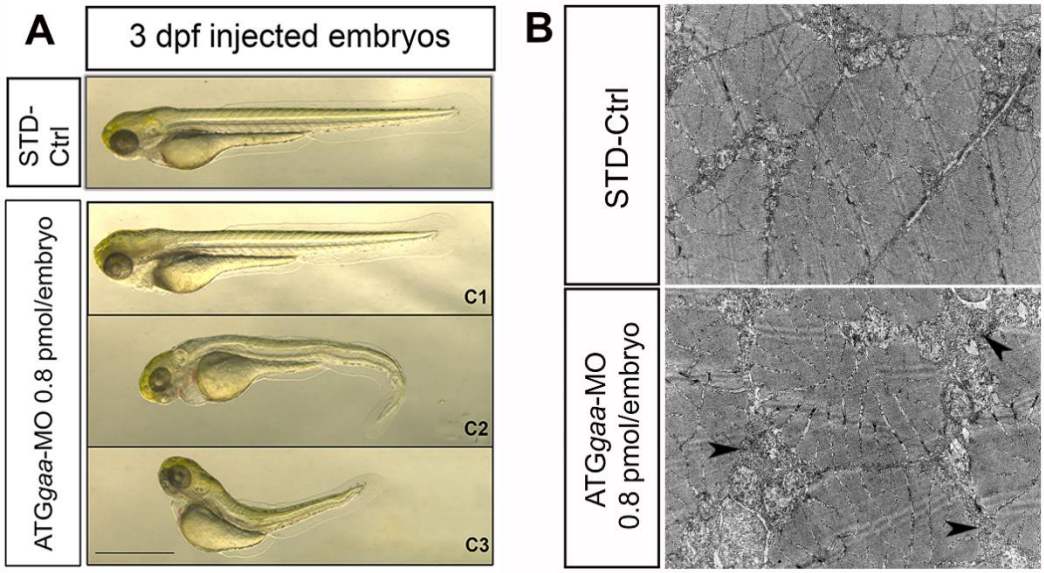

***Fig. 2.5* ATGgaa-MO phenotypes.** *(A) Representative phenotypes at 3 dpf after injection of ATGgaa-MO at a dose of 0.8 pmol/embryo. Phenotypes are divided into C1, C2 and C3 classes. Scale bar = 200 µm. (B) Electron micrographs showing increase in glycogen and vesicles (arrowheads) in ATGgaa morphants, but not in STD-Ctrl embryos. Scale bar = 2µm.*

whereas, of the embryos injected with I9E10gaa-MO, 225 (53% of total) were belonging to the C1 class, 121 (29% of total) to the C2 class, and 74 (18% of total) embryos to the C3 class (Fig. 2.6A, B). Of note, in the I9E10gaa-MO morphants belonging to the C2 class (121 embryos in total), features such as cardiac edema (in 56 morphants), enlargement of the IV cerebral ventricle (in 45 morphants) or both alterations (in 20 morphants) were observed (Fig. 2.6A).

In order to evaluate if knock-down of the gaa was recapitulating the human glycogen storage condition in skeletal muscle, glycogen amount was measured in ATG*gaa*-MO and I9E10*gaa*-MO morphants belonging to the C1 class using a commercial glycogen assay kit. A significant glycogen increase was observed in ATG*gaa* morphants (ATG*gaa*-MO: 72.25 ± 0.323 vs STD-Ctrl: 43.00 ± 0.204; $p<0.0001$), compared to control embryos, which was even greater in I9E10*gaa* morphants (I9E10*gaa*-MO: 122.5 ± 0.540 vs STD-Ctrl: 43.00 ± 0.204; $p<0.0001$) (Figure 2.6C).

In summary injection of both ATG*gaa*-MO and I9E10*gaa*-MO morpholinos caused defects in the embryo morphology and an increase in glycogen content, more marked in the latter.

2.5.1.3 Morphological features were altered in *gaa* knocked down embryos muscle and heart

Toluidine blue-stained transverse and longitudinal semithin sections of ATG*gaa* and I9E10*gaa* morphants, at 4 dpf, showed increased space surrounding muscle fibres, often occupied by blue violet material, not observed in STD-Ctrl embryos (Fig. 2.6D, upper panel). Such blue violet material corresponds to glycogen, which, by Periodic acid–Schiff (PAS) reaction stains fuchsia (Fig. 2.6D, lower panel). At electron microscopy level, increase in glycogen particles, and presence of lysosomal-related elements, such as vesicles, electron dense bodies, and small membranous corpuscles, were observed around muscle fibres in both ATG*gaa* and I9E10*gaa* morphants, more evident in the latter (Fig. 2.6E).

Furthermore, the heart of 4 dpf morphants and control embryos, analyzed at morphological level showed an increase in bluish material in pericardial muscles and an increase in pericardial fluid in I9E10*gaa* morphants, compared to controls (Fig. 2.6F). Moreover, morphant's heart revealed laxity of the ventricle and an augment of the cardiac jelly layer (Fig. 2.6F, b''), compared to the control embryo heart.

In summary, in both morphants glycogen appeared increased by PAS and toluidine blue staining; glycogen particle increase and lysosomal-related elements were observed by electron microscopy; and morphological defects were found in the heart.

2.5.1.4 Lysosomal content was more increased in ATG*gaa* than in I9E10*gaa* morphants

To track lysosomes in vivo, LysoTracker dye was added to ATG*gaa*-MO-, I9E10*gaa*-MO-and STD-Ctrl-MO-injected embryos at 24 hpf. All embryos had been previously injected with 2-NBDG at one cell stage. 2-NBDG, a D-glucose fluorescent derivative used to monitor glucose incorporation into glycogen [118], was used to label glycogen in vivo.

Quantitation of the LysoTracker red signal showed that ATG*gaa* morphants had a significant red signal increment compared to STD-Ctrl (ATG*gaa*-MO:

12360 ± 3195 vs STD-Ctrl: 5154 ± 885.8; p=0.0289), while I9E10*gaa* morphants displayed a red signal comparable to STD-Ctrl (I9E10*gaa*-MO: 6070 ± 837.0 vs STD-Ctrl: 5154 ± 885.8; p=0.4588) (Fig. 2.6G).

Quantitation of the 2-NBDG green signal showed a significant increase in the green dot area in both *gaa* morphants, compared to STD-Ctrl (ATG*gaa*-MO: 5261 ± 702.7 vs STD-Ctrl: 3300 ± 377.0; p= 0.0200; I9E10*gaa*-MO: 6077 ± 851.9 vs STD-Ctrl: 3300 ± 377.0; p=0.0023) (Fig. 2.6H).

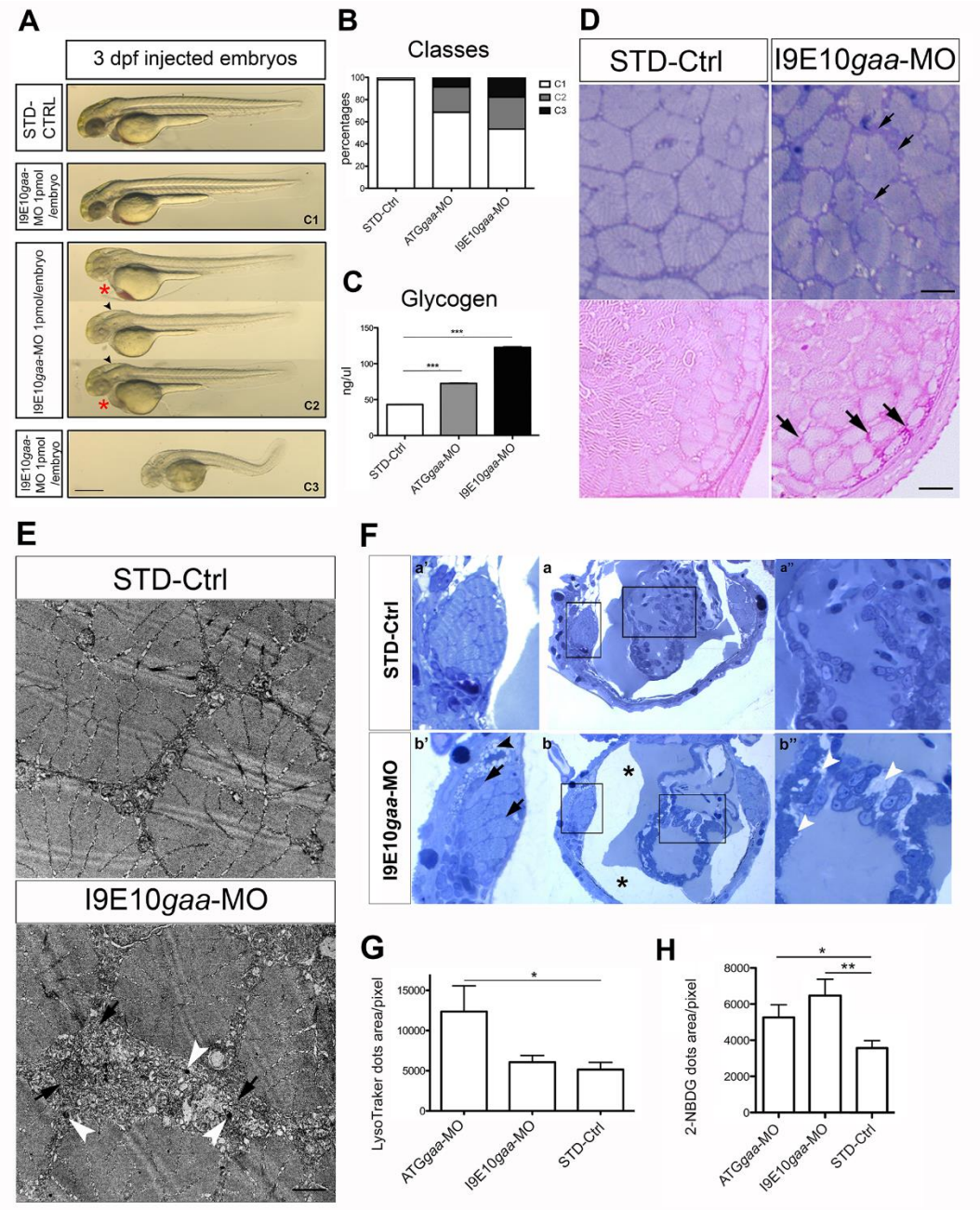

***Fig. 2.6* gaa zebrafish morphants recapitulate the human Pompe disease phenotype.** *(A) Classes of phenotypes shown for the I9E10gaa-injected embryos (C1, C2 and C3). In morphants belonging to class C2, features such as cardiac edema (red asterisk),*

enlargement of the IV cerebral ventricle (black arrowhead) or both alterations are visible. Morphants of the class C1 appear normal, while those of class C3 show disrupted morphology. Scale bar = 300 µm. (B) Percentages of classes obtained with ATGgaa and I9E10gaa morpholinos injections. (C) Glycogen amount measured by the Glycogen Assay kit II in ATGgaa-MO and I9E10gaa-MO morphants pertaining to the C1 class. (D, upper panel) Toluidine blue-stained transverse semithin sections of I9E10gaa morphants showing increased spaces surrounding muscle fibres (black arrows), not observed in STD-Ctrl embryos. Scale bar = 20 µm. (D, lower panel) Periodic Acid Shiff (PAS) staining on transverse semithin sections of STD-Ctrl embryo, compared to I9E10gaa morphant at 4 dpf. Glycogen detected in spaces surrounding muscle fibers (black arrows) is increased and more visible in morphants, compared to controls. Scale bar = 2µm. (E) Electron micrographs showing increase in glycogen (black arrows) and lysosomal corpuscles (white arrowheads) in I9E10gaa morphants, but not in STD-Ctrl embryos. Scale bar = 2µm. (F) Toluidine blue-stained transverse semithin sections of STD-Ctrl embryo heart (a) compared to I9E10gaa morphant heart (b) at 4 dpf. Increased spaces surrounding pericardial muscle fibres (black arrows) and lipid droplets (black arrowhead) are present in morphants, but not in controls (b'). Moreover, an augment of the cardiac jelly layer is observed in the morphant heart (b") (white arroheads), with the presence of an increased cardiac fluid (b) (asterisks). Scale bar = 100 µm. (G) Quantitation of the LysoTracker red signal; and (H) of the 2-NBDG green signal in both morphants and in STD-Ctrl. Results were achieved from 5 independent experiments each using 25 ATGgaa morphants, 25 I9E10gaa morphants and 25 STD-Ctrl embryos.

Tracking in vivo of lysosomes and glycogen by fluorescent dyes showed increase in lysosomes only in ATG*gaa* morphants, while glycogen was increased in both.

2.5.1.5 Motility was defective in *gaa* knocked down embryos

The touch evoked response test was performed on ATG*gaa* and I9E10gaa morphants belonging to the C1 class at 3 dpf. In comparison to STD-Ctrl-injected embryos, a slight escape attempt was present in 21 ATG*gaa* morphants out of 30, with evident muscle stiffness. Motility defects were more severe in I9E10*gaa* morphants: 26 injected embryos out of 30 showed very weak escape contraction, and obvious muscle stiffness.

2.5.1.6 Expression of autophagy-related transcripts and proteins was altered in I9E10*gaa* morphants

At 48 hpf, *atg7, atg4, beclin1, mTor, p62, lc3b* and *ulk1* transcript levels by qRT-PCR were not significantly different in ATG*gaa* morphants compared to STD-Ctrl embryos (Fig. 2.7). In I9E10*gaa* morphants a significant increase in lc3b (I9E10*gaa*-MO: 2.284 ± 0.297 vs STD-Ctrl: 0.9998 ± 0.225; p=0.0138) and beclin1 transcript levels (I9E10*gaa*-MO: 2.259 ± 0.301 vs STD-Ctrl: 1.015 ± 0.102; p=0.0078) was observed, compared to STD-Ctrl (Fig. 2.8A).

Proteins related to autophagy Lc3, p62, mTOR, p-mTOR, AMPk, p-AMPk, Lamp2 and Beclin1, quantitated on Western blot bands, at 24 hpf, were not significantly different in both morphants compared to STD-Ctrl embryos (Fig. 2.9); whereas, in I9E10*gaa* morphants, at 4 dpf, p62 (I9E10*gaa*-MO: 1.037 ± 0.2109 vs STD-Ctrl: 0.2733 ± 0.05925; p=0.0252) and Lc3b (measured as ratio Lc3bII/Lc3bI) (I9E10*gaa*-MO: 1.790 ± 0.01155 vs STD-Ctrl: 0.8600 ± 0.05568; p<0.0001) were significantly increased compared to STD-Ctrl (Fig. 2.8B).

In summary, among autophagy-related transcripts and proteins, *lc3b* and *beclin1* mRNA levels were significantly increased at 48hpf, and p62 and Lc3b proteins were significantly increased at 4dpf in I9E10*gaa*, but not in ATG*gaa* morphants.

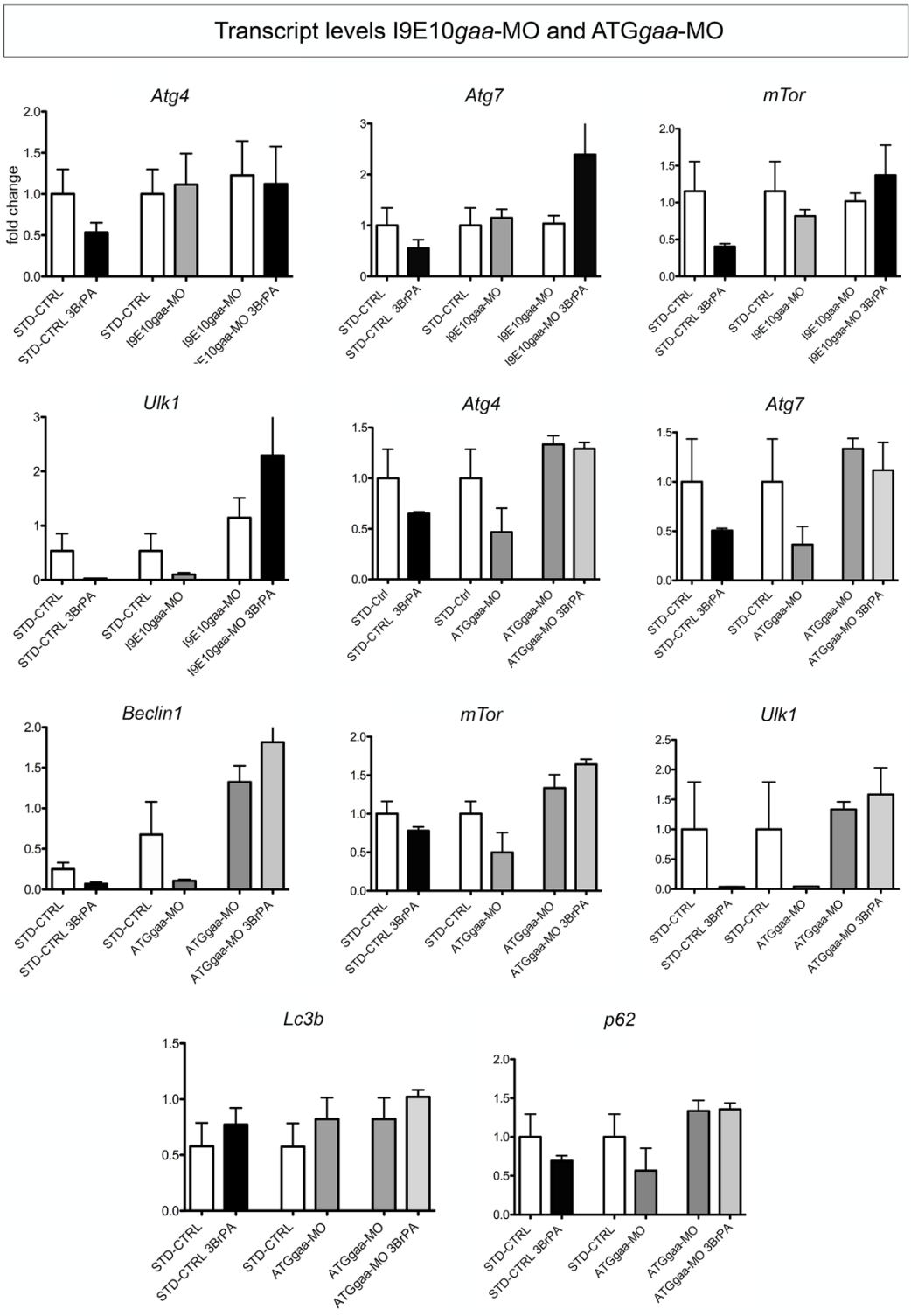

Fig. 2.7 ***Graphs of autophagy-related transcript levels in morphants and control embryos, pre- and post- 3-BrPa treatment.*** *Transcript levels that did not differ significantly from STD-Ctrl are shown for both morphants at 48 hpf.*

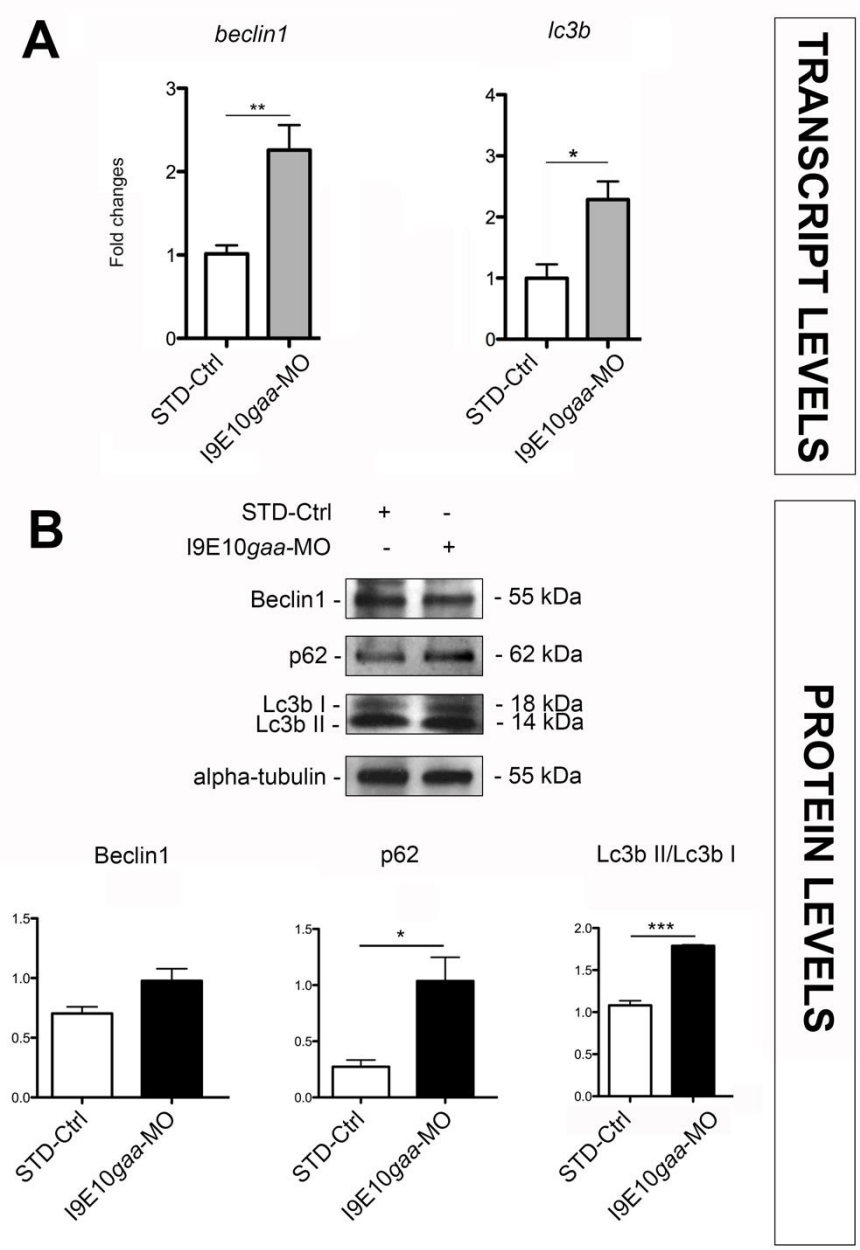

Fig. 2.8 ***Expression of autophagy related transcripts and proteins.*** *(A) beclin1 and lc3b transcript levels at 48 hpf. (B) Representative western blot showing Beclin1, p62 and Lc3b protein bands; and their quantitation (average of 3 gels) at 4 dpf, in I9E10gaa morphants compared to STD-Ctrl. Results were achieved from 5 independent experiments each using cDNA obtained after RNA extraction from 10 embryos pulled together, for a total of 50 embryos.*

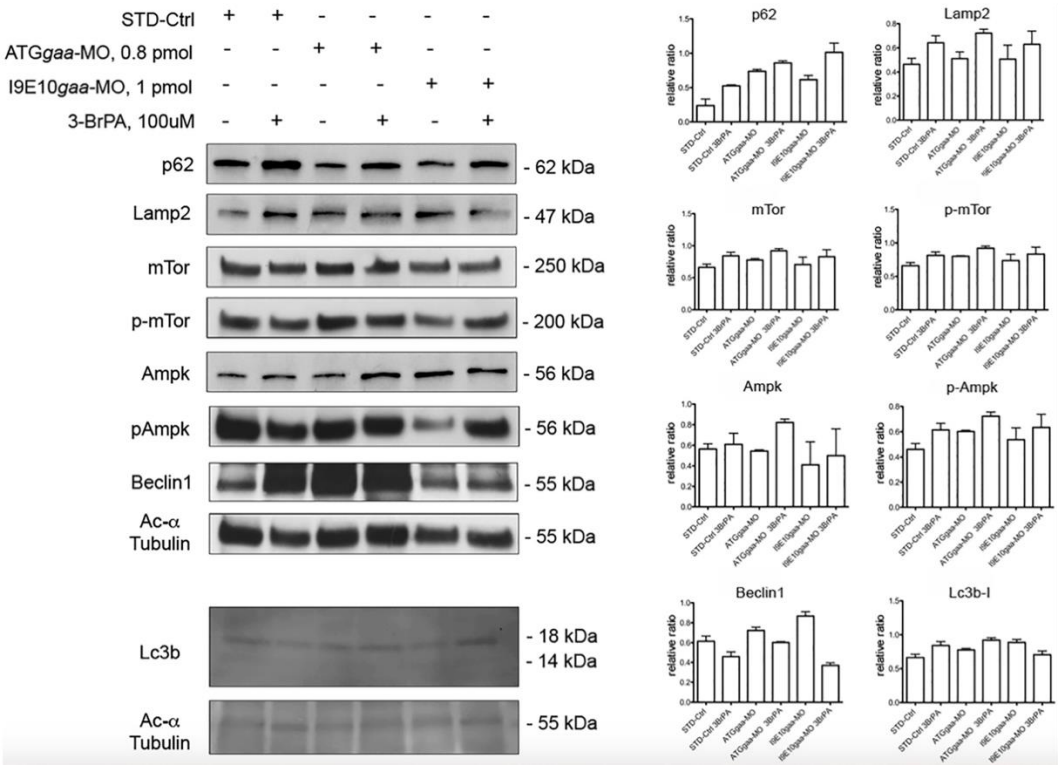

Fig. 2.9 ***Western blot of autophagy-related proteins, in morphants and control embryos, at 24 hpf, pre- and post- 3-BrPa treatment.*** *At 24 hpf, proteins related to autophagy Lc3b, p62, mTor, p-mTor, AMPk, p-AMPk, Lamp2 and Beclin1, quantitated on western blot bands, were not significantly different in both morphants compared to STD-Ctrl embryos. Note that in zebrafish Lc3b II starts to be synthetized at 24 hpf, therefore it is detectable only after 26 hpf.*

2.5.1.7 *gaa* mRNA injection rescued Pompe disease phenotype in I9E10*gaa* morphants

To avoid base-pairing between the oligomer and the in vitro synthetized mRNA that could occur with ATG*gaa* morpholinos, the rescue experiment was performed exclusively in I9E10*gaa* morphants (hereinafter called rescued I9E10*gaa* morphants). One-cell stage embryos were co-injected with I9E10*gaa*-MO (1 pmol/embryo) and 10pg/4nL *gaa* mRNA.

The resulting phenotypes were compared with I9E10*gaa* morphants and with STD-Ctrl embryos and the distribution of the phenotypes, based on the correct formation of somites, was annotated at 24 hpf (Fig. 2.9A). To classify the phenotypes, correct morphology (Fig. 2.9Ba), developmental delay (Fig. 2.9Bc) and deformities (Fig. 2.9Be) were considered. The rescued morphants presented a significant increase in the number of embryos with

correct morphology, compared to non-rescued I9E10*gaa*-MO (I9E10*gaa*-MO + *gaa* mRNA: 14.80 ± 1.158 vs I9E10*gaa*-MO: 6.200 ± 0.8602; p=0.0003). No significant differences were observed in growth retardation between rescued and non-rescued I9E10*gaa* morphants; while deformities were significantly less in rescued I9E10*gaa* morphants compared to non-rescued (I9E10*gaa*-MO + *gaa* mRNA: 5.0 ± 0.3162 vs I9E10*gaa*-MO: 12.60 ± 2.379; p=0.0133) (Fig. 2.9B, C).

The embryos were then let develop in fresh fish water and again observed at 48 hpf. At this developmental stage, although the I9E10*gaa* morphants presented fewer morphological defects, rescued morphants still showed significantly higher numbers of embryos presenting an appropriate body and somite formation (Fig. 2.9Bb) (I9E10*gaa*-MO + *gaa* mRNA: 18.20 ± 2.672 vs I9E10*gaa*-MO: 10.40 ± 1.860; p=0.0435). Numbers of morphants with growth retardation (Fig. 2.9Bd) or deformities (Fig. 2.9Bf) were not significantly different between rescued and non-rescued morphants at this developmental stage. Rescued morphants presenting cardiac edema, enlargement of the IV cerebral ventricle or both, were fewer than non-rescued morphants, but, again, the difference was not significant.

Rescue with *gaa* mRNA on glycogen storage was assessed by the glycogen assay kit at 48 hpf. The amount of glycogen (ng/µl) was significantly less in I9E10*gaa* rescued morphants, compared to non-rescued I9E10*gaa*-MO morphants (I9E10*gaa*-MO + *gaa* mRNA: 143.6 ± 0.731 vs I9E10*gaa*-MO: 155.3 ± 2.186; p=0.0071) (Fig. 2.9D).

In summary, the rescue experiment showed that embryos with correct morphology were more than non-rescued embryos at 24 hpf, and at 48 hpf, although at the latter stage growth retardation or deformities did not differ. Glycogen amount was also significantly less in rescued morphants.

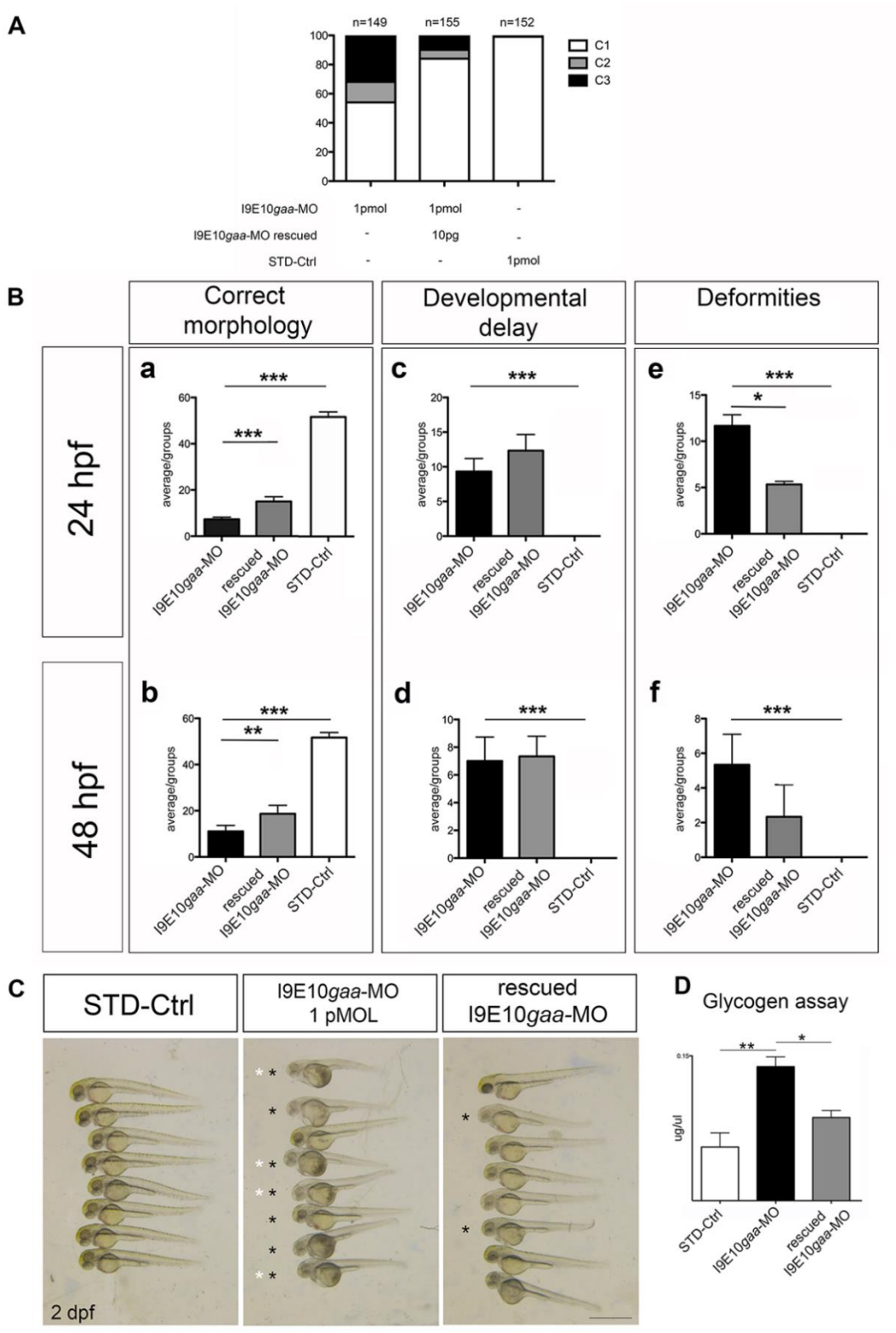

***Fig. 2.9* Rescue of I9E10gaa morphants phenotype.** *(A) Classes of phenotypes obtained at 24 hpf after co-injection of I9E10gaa-MO (1 pmol/embryo) and 10pg/4nL gaa mRNA. (B) Graphs reporting average numbers of embryos with correct morphology (a, b), developmental delay (c, d) and deformities (e, f) at 24 hpf and 48 hpf. The total number of embryos per group were: n=59 I9E10gaa-MO, n=73 rescued I9E10gaa-MO, n=78 3-BrPA*

rescued I9E10gaa-MO, n=62 I9E10gaa-MO plus 3-BrPA, n=60 STD Ctrl. (C) Representative phenotypes of STD-Ctrl, I9E10gaa-MO and I9E10gaa rescued embryos, at 2 dpf, with cardiac edema (black asterisks) and enlargement of IV hindbrain ventricle (white asterisks) more evident in I9E10gaa morphants. Scale bar = 200 µm. (D) Evaluation of glycogen amount in I9E10gaa morphants before and after rescue, compared to STD-Ctrl, at 48 hpf. Results were achieved from 4 independent experiments, each using 10 embryos pulled together, for a total of 40 embryos.

2.5.2.1 3-BrPA enhanced motility behavior in *gaa* morphants

The touch evoked response test, performed at 3 dpf on 3-BrPA-treated ATG*gaa* and I9E10*gaa* morphants, showed an improvement of escape contractions in both morphants (I9E10*gaa*-MO: n=20/30; ATG*gaa*-MO: n=24/33) compared to untreated morphants (n=30/30) (Fig. 2.10).

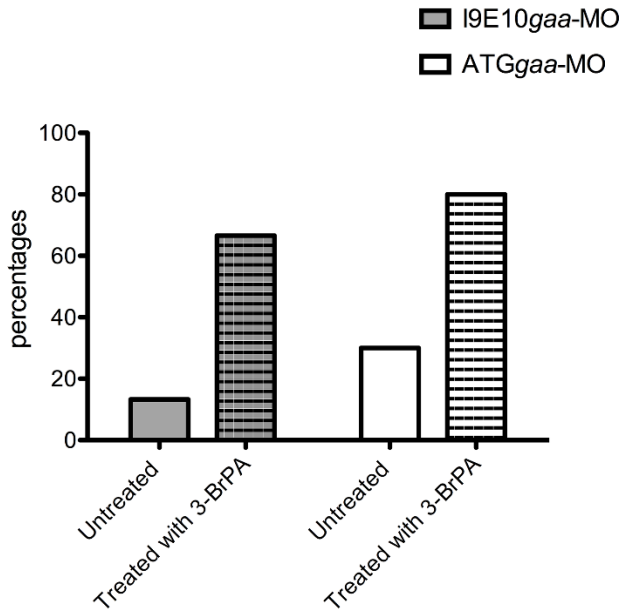

***Fig. 2.10* Quantitation of motility amelioration after 3-BrPA treatment.** *Graph showing an improvement of motility after 3-BrPA treatment in I9E10gaa and in ATGgaa morphants.*

2.5.2.2 3-BrPA improved muscle morphology in morphants

In transverse and longitudinal semi thin sections of ATG*gaa* and I9E10*gaa* morphants at 4 dpf treated with 3-BrPA, the space surrounding muscle fibres appeared either reduced compared to untreated morphants, as shown in toluidine blue-stained semi thin sections (Fig. 2.11A, D) or devoid of positive fuchsia material, as shown in PAS-stained sections (Fig. 2.11B, ,E). At the electron microscopy level reduction in glycogen particles and presence of empty spaces around fibers was observed in both ATG*gaa* and I9E10*gaa* 3-BrPA-treated morphants (Fig. 2.11C, F).

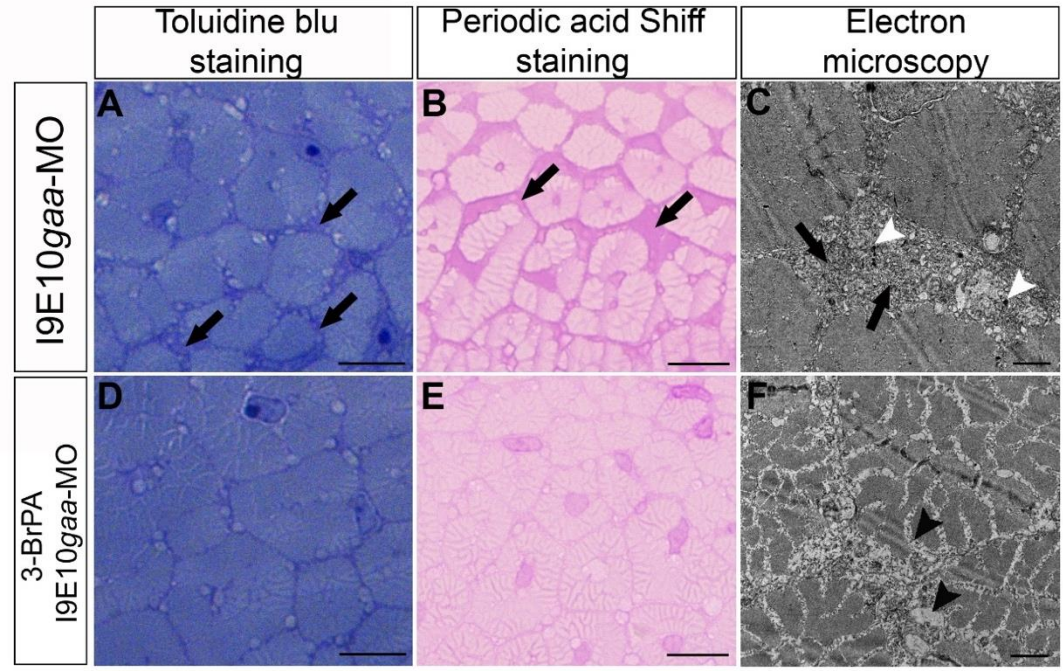

***Fig. 2.11* Effect of 3-BrPA treatment on muscle morphology.** *(A, D) Toluidine blue- and (B, E) PAS-stained transverse semi thin sections of I9E10gaa-MO embryos at 4 dpf, showing that, after 3-BrPA treatment, spaces surrounding muscle fibres (arrows) appear either reduced or devoid of positive fuchsia material around muscle fibres. Scale bars = 20 µm. (C, F) Electron micrographs showing that glycogen particles (black arrows) present in I9E10gaa morphants (C), appear decreased after 3-BrPA treatment (F), while empty spaces around fibres (black arrowheads) appear increased. Lysosomal corpuscles (white arrowheads) are visible in untreated I9E10gaa morphants. Scale bar = 2µm.*

2.5.2.3 3-BrPA increased lysosomal content in morphants

Quantitation of LysoTracker (Fig. 2.12A) red signal showed a significant increase in the red signal in ATG*gaa* morphants treated with 100 μM 3-BrPA, compared to untreated ATG*gaa*-MO (ATG*gaa*-MO + 3-BrPA: 45910 ± 8922 vs ATG*gaa*-MO: 12360 ± 3195; p=0.0011), as well as in I9E10*gaa*-MO treated morphants compared to untreated (I9E10*gaa*-MO + 3-BrPA: 15590 ± 3575 vs I9E10*gaa*-MO: 6070 ± 837.0; p=0.0175) (Fig. 2.12B).

Quantitation of 2-NBDG showed in both 3-BrPA-treated morphants a significant decrease in the signal compared to untreated morphants (ATG*gaa*-MO + 3-BrPA: 3300 ± 377.0 vs ATG*gaa*-MO: 5261± 702.7; p=0.0200; I9E10*gaa*-MO + 3-BrPA: 2470 ± 217.2 vs I9E10*gaa*-MO: 6077 ± 851.9; p<0.0001) (Fig. 2.12C).

Tracking in vivo of lysosomes and glycogen by fluorescent dyes showed an increase in lysosome content and a decrease in glycogen in both morphants after 3-BrPA treatment.

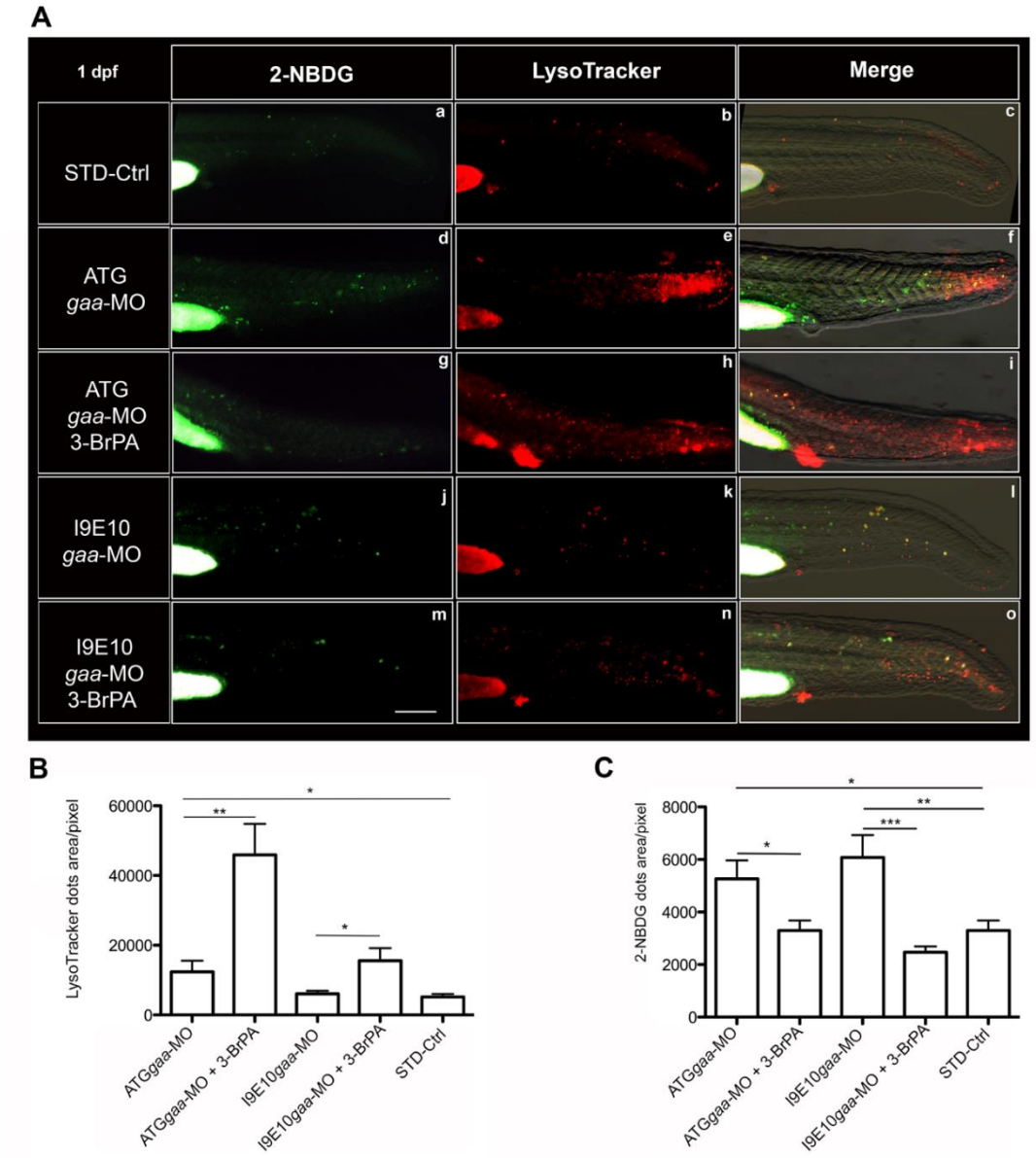

Fig. 2.12 ***3-BrPA treatment effect on lysosomes.*** *(A) Fluorescence images showing LysoTracker and 2-NBDG signals in STD-Ctrl (a-c), ATGgaa-MO injected embryos (d-f), ATGgaa-MO 3-BrPA-treated embryos (g-i), I9E10gaa-MO injected embryos (j-l), I9E10gaa-MO 3-BrPAtreated embryos (m-o). Scale bar = 100 µm. (B, C) Quantitation of LysoTracker and 2-NBDG signal in ATGgaa and I9E10gaa morphants before and after 3-BrPAtreatment, and in STD-Ctrl embryos. The LysoTracker dye and 2-NBDG assessment was performed in 23 zebrafish embryos per group (115 embryos in total), obtained from 5 independent experiments.*

2.5.2.4 3-BrPA treatments improved rescue in I9E10*gaa* morphants

3-BrPA treatments were assessed after rescue in I9E10*gaa* morphants as the rescue experiment was carried out only in those embryos. At 24 hpf a significant increase in the number of embryos presenting with correct morphology was observed in morphants rescued with *gaa* mRNA and treated with 3-BrPA compared to untreated and rescued morphants (I9E10*gaa*-MO + mRNA + 3-BrPA: 25.670 ± 1.856 vs I9E10*gaa*-MO + mRNA: 15.00 ± 2.082; p=0.0187); or compared to untreated morphants (I9E10*gaa*-MO + mRNA + 3-BrPA: 25.670 ± 1.856 vs I9E10*gaa*-MO: 7.333 ± 0.882; p=0.0009).

Furthermore, the number of embryos presenting correct morphology was increased in I9E10*gaa*-MO + 3-BrPA compared to I9E10*gaa*-MO embryos (I9E10*gaa*-MO + 3-BrPA: 16.00 ± 2.082 vs I9E10*gaa*-MO: 7.333 ± 0.8819; p=0.0186) (Fig. 2.13Aa, Ab).

Numbers of embryos showing growth retardation were not significantly different between groups (I9E10*gaa*-MO, rescued I9E10*gaa*-MO, and rescued I9E10*gaa*-MO + 3-BrPA).

In the rescued morphants treated with 3-BrPA, those carrying deformities were significantly fewer than in the non-rescued and untreated morphants (I9E10*gaa*-MO: 11.67 ± 1.202 vs I9E10*gaa*-MO + mRNA + 3-BrPA: 3.667 ± 1.856; p=0.0224), but similar to the rescued morphants (I9E10*gaa*-MO + mRNA + 3-BrPA: 1.667 ± 0.8819 vs I9E10*gaa*-MO + mRNA: 2.333 ± 1.856; p=0.7619).

The embryos treated with 3-BrPA alone presented a significant lower number of embryos carrying deformities than I9E10gaa morphants (I9E10*gaa*-MO + 3-BrPA: 4.667 ± 0.3333 vs I9E10*gaa*-MO: 11.67 ± 1.202; p=0,0050) (Fig. 2.13Ac).

At 48 hpf, the number of morphants with correct morphology was significantly higher in the rescued morphants and 3-BrPA-treated compared to untreated and rescued morphants (I9E10*gaa*-MO + mRNA + 3-BrPA: 33.00 ± 3.215 vs I9E10*gaa*-MO + mRNA: 18.67 ± 3.667; p=0.0424), or compared to untreated and non-rescued morphants (I9E10*gaa*-MO +

mRNA + 3-BrPA: 33.00 ± 3.215 vs I9E10gaa-MO: 11.00 ± 2.646; p=0.0062) (Fig. 2.13Bb).

Differences in growth retardation and in deformities were not significant between groups at 48 hpf (Fig. 2.13Ad, Af).

3-BrPA treatment of rescued I9E10*gaa* morphants significantly reduced numbers of embryos presenting cardiac edema and hindbrain IV ventricle enlargement, at 48 hpf, compared to untreated morphants (Fig. 2.13B,C). In particular, in rescued and 3-BrPA treated morphants, numbers of embryos presenting cardiac edema were significantly fewer (2,2%, n=78) than in untreated and non-rescued morphants (20,3%, n=59); moreover, hindbrain enlargement was totally absent (0%, n=78) compared to untreated and non-rescued morphants (7,5%, n=59). Moreover, morphants treated with 3-BrPA alone showed a significant decrease (2,7%, n=62) in embryos percentage presenting cardiac edema and hindbrain IV ventricle enlargement, compared to untreated and non-rescued morphants (20,3%, n=59).

3-BrPA treatment of rescued I9E10gaa morphants did not change glycogen amount, at 48 hpf, compared to untreated and rescued I9E10*gaa* morphants (I9E10*gaa*-MO + mRNA + 3-BrPA: 139.2 ± 0.441 vs I9E10*gaa*-MO + mRNA: 143.6 ± 0.731; p=0.064). The 3-BrPA treatment alone reduced glycogen amount significantly, compared to the glycogen present in I9E10*gaa* morphants (I9E10*gaa*-MO + 3-BrPA: 0.1420 ± 0.001528 vs I9E10*gaa*-MO: 0.1487 ± 0.001202; p=0,0265) (Fig. 2.13D).

In summary, 3-BrPA treatment improved the overall morphology and the cardiac edema in I9E10*gaa* morphants either alone or in addition to rescue. The rescue of I9E10*gaa* embryos reduced glycogen amount, in a comparable manner to 3-BrPA treatment.

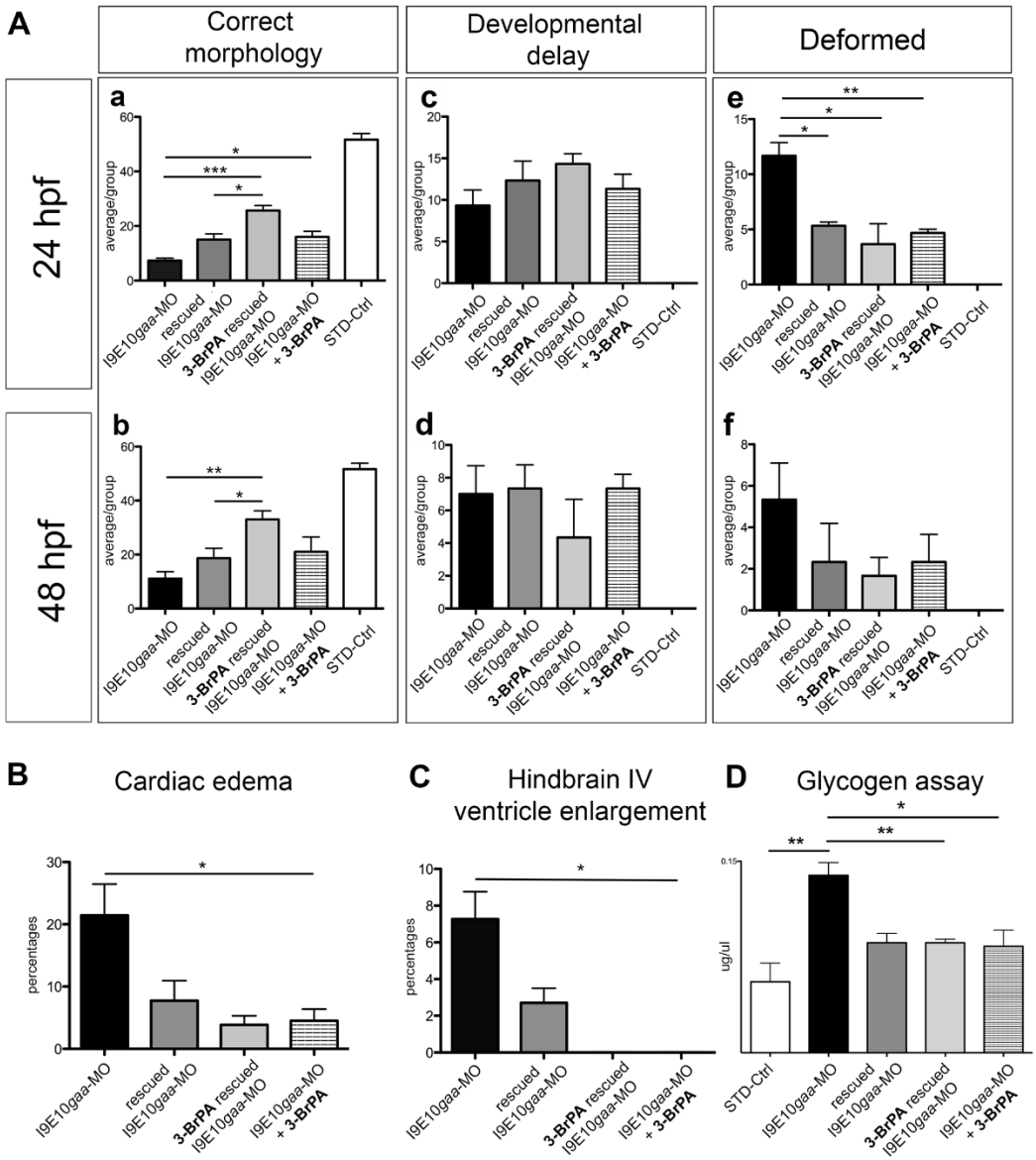

***Fig. 2.13* 3-BrPA treatment effect on rescue experiment.** *(A) Graphs reporting average numbers of embryos with correct morphology (a, b), developmental delay (c, d) and deformities (e,f) at 24 hpf and 48 hpf, showing improvement of phenotypes after 3-BrPA-treatment in embryos either rescued or non-rescued. The total number of embryos per group were: n=59 I9E10gaa-MO, n=73 rescued I9E10gaa-MO, n=78 3-BrPA rescued I9E10gaa-MO, n=62 I9E10gaa-MO plus 3-BrPA, n=60 STD Ctrl. (B, C) Percentages of I9E10gaa morphants presenting cardiac edema or hindbrain IV ventricle enlargement after rescue, after rescue plus 3-BrPA treatment, and after 3-BrPA alone. The total number of embryos per group were: n=59 I9E10gaa-MO, n=73 rescued I9E10gaa-MO, n=78 3-BrPA rescued I9E10gaa-MO, n=62 I9E10gaa-MO plus 3-BrPA. (D) Glycogen amount in I9E10gaa morphants, after rescue, after rescue plus 3-BrPA treatment, and after 3-BrPA alone. Results were achieved from 4 independent experiments, each using 10 embryos pulled together, for a total of 40 embryos per group.*

2.5.2.5 3-BrPA treatment modified the expression of *Beclin1, p62*, and *Lc3b* transcripts and proteins

3-BrPA treatment did not significantly change *atg7, atg4, mtor, p62, lc3b* or *ulk1* transcripts levels in ATG*gaa* morphants and STD-Ctrl embryos compared to untreated.

3-BrPA-treatment significantly increased transcript levels of *lc3b* (I9E10*gaa*-MO + 3-BrPA: 3.298 ± 0.1572 vs I9E10*gaa*-MO: 2.284 ± 0.2973, p=0.0235), and *p62* (I9E10*gaa*-MO + 3-BrPA: 5.593 ± 0.6959 vs I9E10*gaa*-MO: 1.009 ± 0.07910, p=0.0006), and significantly decreased transcript levels of *beclin1* (I9E10*gaa*-MO + 3-BrPA: 0.3567 ± 0.2024 vs I9E10*gaa*-MO: 1.024 ± 0.1364, p=0.0357) in I9E10*gaa* morphants compared to untreated I9E10*gaa* morphants (Fig. 2.14A).

A significant decrease in *beclin1* mRNA level was also observed in 3-BrPA-treated STD-Ctrl embryos compared to untreated STD-Ctrl embryos (STD-Ctrl + 3-BrPA: 0.341 ± 0.04 vs STD-Ctrl: 1.015 ± 0.102; p=0.0008).

3-BrPA-treatment significantly decreased Beclin1 protein amount in I9E10*gaa* morphants compared to untreated I9E10gaa morphants (I9E10*gaa*-MO: 0.9767 ± 0.1014 vs I9E10*gaa*-MO + 3-BrPA: 0.4833 ± 0.04096; p=0.0107).

3-BrPA-treatment significant increased p62 protein amount (STD-Ctrl + 3-BrPA: 0.6133 ± 0.01202 vs STD-Ctrl: 0.2733 ± 0.05925; p=0.0049) and significantly decreased Lc3b (STD-Ctrl + 3-BrPA: 1.117 ± 0.06489 vs STD-Ctrl: 0.8600 ± 0.05568; p=0.0399) in STD-Ctrl embryos compared to untreated STD-Ctrl (Fig. 2.14B).

3-BrPA treatment main effect was an increase in *p62* and a decrease in *beclin1* mRNA levels and Beclin1 protein amount in I9E10*gaa* morphants. It also induced a decrease in *beclin1* mRNA, and an increase in p62 and decrease in Lc3b protein amount in STD-Ctrl.

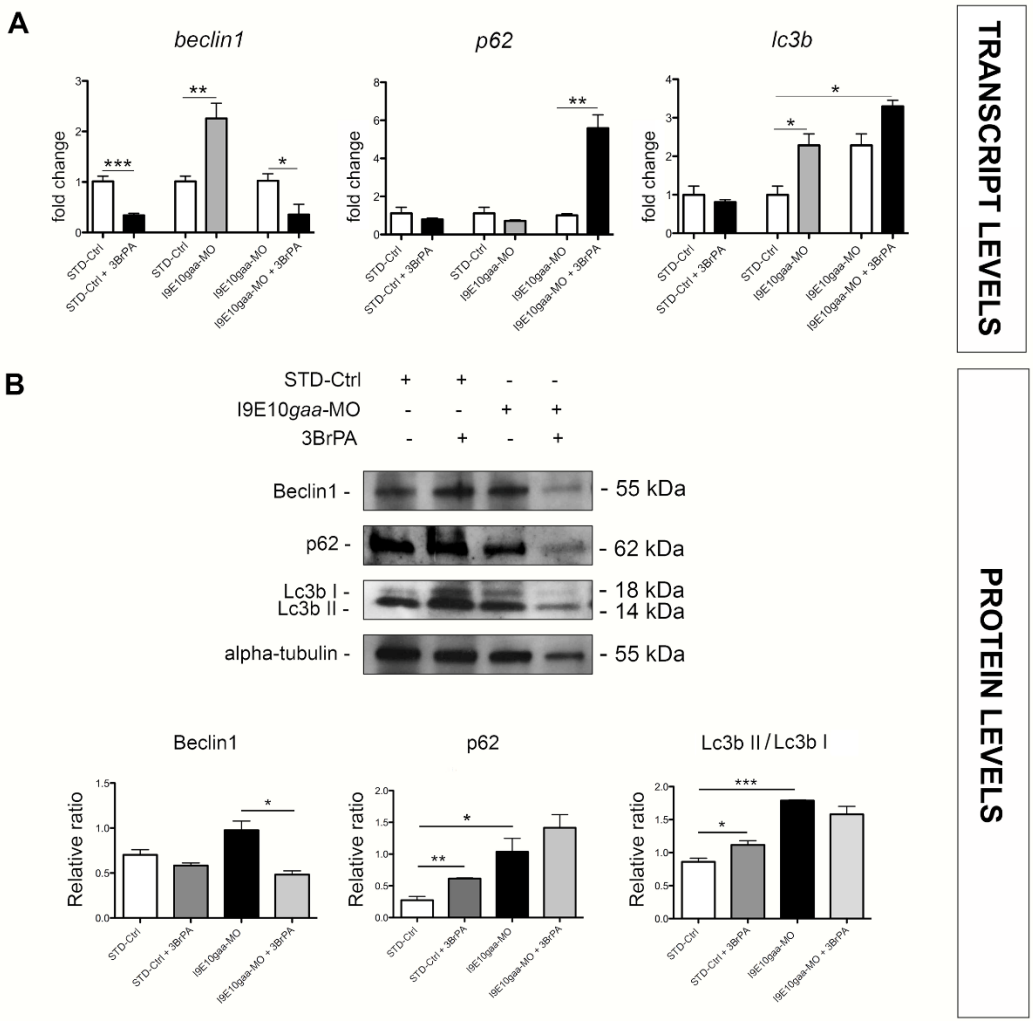

***Fig. 2.14* Effects of 3-BrPA on autophagy-related transcripts and proteins in I9E10gaa morphants.** *(A) beclin1, p62 and lc3b transcript levels; and (B) representative western blot showing Beclin1, p62 and Lc3b protein bands; and their quantitation (average of 3 gels) at 4 dpf, in I9E10gaa morphants and STD-Ctrl embryos before and after 3-BrPA treatment. Results were achieved using cDNA obtained after RNA extraction from 10 embryos pulled together, collected during 5 independent experiments, for a total of 50 embryos.*

2.6 Discussion

Currently, the standard of care for Pompe disease patients is ERT which is efficacious in improving cardiomyopathy but not equally effective in cases with involvement of skeletal muscle: therefore, improved or supplementary therapeutic strategies are needed.

In our study, we have generated and characterized a new transient Pompe disease zebrafish model aimed at testing novel potential remedies for this pathology.

Taking advantage of two different morpholinos, one directed against the translation start site of the *gaa* transcript, and one targeting the splice site between intron 9 and exon 10, close to the catalytic site of the protein, we obtained the ATG*gaa* morphants, expressing low amount of the Gaa protein, and the I9E10*gaa* morphants, in which an aberrant *gaa* transcript and protein is present. Such aberrant protein, of theoretically lower molecular weight (57-58 kDa, compared to circa 70 kDa WT), was not detected by western blot. We presume that this truncated form deriving from the translation of the aberrant mRNA with intron retention in I9E10gaa morphants, acts as a dominant negative. Although the aberrant cDNA is clearly visible, as shown in Supplementary Figure 4B, the anti-Gaa antibody cannot possibly detect a truncated version of the protein, as the only conserved epitope in zebrafish is located at the C-terminus of the protein. Our extensive investigation shows that several pathological characteristics recapitulate Pompe disease features [119] in both models, but especially in the I9E10*gaa*-MO-injected embryos.

We found an increase in glycogen content, detected using two different methods: one based on injection of 2-NBDG, that allows visualization of the glucose flux in 24 hpf zebrafish embryos by fluorescence microscopy analysis [120]; and one based on colorimetric analysis with a commercial assay kit tailored to our animal model. Both approaches showed a significant increment in glycogen amount in Pompe disease

zebrafish knockdown models, more evident in the I9E10gaa morphants. The increment was rescued by co-injection with *gaa* mRNA confirming that Gaa deficiency was the cause of glycogen increase. These data were

confirmed also by the morphological studies at optical and ultrastructural level.

We observed heart edema in almost half of the embryos among the I9E10gaa morphants at 48 hpf, that we associated with the Pompe disease phenotype. This was confirmed by the morphological analysis of the heart of 4 dpf glutaraldehyde-fixed morphants and control embryos. In I9E10*gaa* morphants, compared to controls, we observed an increase in glycogen surrounding the pericardial muscles fibers and an increased amount of fluid in the pericardial cavity (edema), likely caused by the malfunction of the pericardial muscles. Moreover, morphants showed an abnormal deposition of the cardiac jelly layer, located between endocardium and myocardium [121]. Cardiac failure is the main cause of death in untreated classic infantile Pompe disease, but is also a characteristic of some late onset Pompe disease patients [122]. Edema of the heart, in some cases, has been associated to off target effects of morpholino in zebrafish. However, in our model, the edema was proportionate to the severity of the phenotypes and, importantly, *gaa* reintroduction during the rescue experiment ameliorated this particular aspect confirming that Gaa deficiency was the exclusive cause of the edema.

Furthermore, we observed reduced morphant motility, more marked in the I9E10*gaa* morphants, due to altered functionality of embryo muscles. This aspect was recovered during the rescue experiment, again confirming that Gaa deficiency, with consequent increment of glycogen storage, was the cause of the failed touch evoked response test.

Finally, in our knockdown model, we also found altered expression of autophagy-related components. In particular, we observed an increase in lysosomal corpuscles at ultrastructural level, a significant increase in lysosomal content (by LysoTracker staining), and a significantly increased expression of autophagy-related transcripts and proteins, with some differences between the two morphants.

The wide spectrum of Pompe disease is indeed attributed to altered autophagic flux, although it remains unclear how, since it is yet unknown if an excessive acceleration or reduction of this process is present. In addition to being involved in degradation, autophagy plays an important part in

inflammation and pathogen clearance, and is implicated in cellular architectural changes that occur during differentiation and development [123]. Since autophagy is a fundamental evolutionarily conserved mechanism, and zebrafish development is strongly connected with it [109,124], we associated the developmental retardation, more evident in our I9E10gaa morphants, to altered autophagy [125]. Indeed, we observed significant changes in *beclin1* and *lc3b* transcript levels and in p62 and Lc3b protein levels in the I9E10*gaa* morphants. All these proteins are involved in early stages of autophagy: Beclin1 is an autophagy regulator involved in the formation of a double-membrane structure that engulfs cytoplasmic material to form the autophagosomes [126], Lc3b is related to the crescent-shaped double membrane tightly associated to Beclin1, and p62 facilitates ubiquitinated protein degradation by linking the ubiquitin–proteasome system to the autophagy pathway [127]. The lack of correlation between protein levels and mRNA expression is not surprising given that multiple processes contribute to the expression level of a protein [128].

All together our data confirm that knocking down or inducing the insertion of intron 10 in the gaa transcript in zebrafish, recapitulate most aspects of the human Pompe disease condition, which are more evident in the I9E10gaa morphants.

Remarkably, the zebrafish Pompe disease knockdown model, allowed us to evaluate the effects of 3-BrPA *in vivo*. This compound has never been tested before for Pompe disease. Since the main action of this compound is the inhibition of the key glycolytic enzyme HKII, a key regulator of glycolysis through autophagy [129], we hypothesized that 3-BrPA could potentially modulate glycogen accumulation and autophagy in Pompe disease muscle.

The beneficial, but also toxic effects of this compound have been known in the last 10 years in particular for the treatment of glycolysis-dependent tumors [130,131].

In cancer cells, 3BrPA can accomplish its deleterious effect thanks to their high expression of monocarboxylate transporters and exacerbation of glycolytic metabolism [92]; however, 3-BrPA is slightly toxic to cells due to ROS production [91]. To limit such potential adverse effect, we used 3-BrPA

at a concentration (100 μM) that was one-twentieth the concentration (2 mM) identified as LD50.

We observed an improvement in morphants motility after 3-BrPA administration, which we interpreted as due to an improved functionality of embryo muscles, consistent with the decrease in glycogen storage. These data were confirmed also by the morphological studies at optical and ultrastructural level. In addition to its positive action in the I9E10*gaa* morphants, 3-BrPA enhanced the effect of the rescue experiment on glycogen storage, cardiac edema and hindbrain enlargement. Such result suggests that 3-BrPA can correct some of the phenotypic changes seen in the Pompe disease model and could be an adjuvant therapy in combination with ERT since the rescue experiment could mirror in some way the enzymatic replacement therapy.

Furthermore, 3-BrPA treatment induced changes in autophagy-related transcripts and proteins. To this regard, a major result of the treatment was the reduction in Beclin1 transcript and protein, since Beclin1 is central in the early formation of autophagosomes. A reduced nucleation, consequent to Beclin1 decrease, would produce fewer autophagosomes. The subsequent increase in Lc3b and p62 levels instead, is probably related to a slow-down of the autophagic flux and to an increment in size of the autophagosomes.

We also observed an increment in red dots in the LysoTracker dye experiment in I9E10*gaa* morphants after 3-BrPA treatment, resulting in an increase in lysosomes, compared to untreated morphants. 3-BrPA is likely to induce a mild status of starvation that would activate the transcription factor EB (TFEB), the lysosomal biogenesis transcription factor, thereby increasing lysosomal activity (acidification and delivery of hydrolases) and trafficking (autophagosome-lysosome fusion) in strict correlation with autophagy [132].

Moreover, we observed a significant increase in lysosomal content in ATG*gaa* morphants. The meaning of such finding is not clear at present. A possible explanation is that the residual, but normally functioning Gaa protein in the ATG*gaa* model somehow induces the formation of larger lysosomes to contain the excess of glycogen, while the aberrant Gaa protein

in the I9E10*gaa* model might stimulate an early contribution of the complex mechanism of autophagy.

In conclusion, we characterized for the first time a Pompe disease transient model in zebrafish that recapitulates most of the defects observed in human patients and reflects the genetic condition of most Pompe patients, in which the GAA is dysfunctional, but not totally absent.

This model thus has proven to be a suitable, rapid and low cost tool both for investigating pathogenic mechanisms of Pompe disease and for testing compounds with therapeutic potential.

To this regard we have demonstrated, as proof of principle, that 3-BrPA has beneficial effects in the zebrafish Pompe disease model, since it reduces the glucose entrance in muscle cells and modulates the autophagy flux, without creating a problematic condition of starvation. Additional studies will be needed in a stable zebrafish mutant to explore 3-BrPA treatment for a long period of time. The present study is in fact preparatory to the development of a stable zebrafish PD model. In such model the catalytic site of the Gaa protein will be disrupted to better reproduce the pathological features of PD, keeping in mind that a compensation of the pathological phenotype could occur in adult stages, as already reported [133].

Our new zebrafish PD model, will simplify testing novel drugs with therapeutic potential, as 3-BrPA, reducing timing and costs of the screening. Moreover, this translational model, that recapitulates better the patient conditions, will accelerate further investigations that underlies glycogen storage conditions.

3

Conclusions

3.1 Zebrafish transient model and novel therapies for Pompe disease

Zebrafish revealed to be a powerful animal model to study Pompe disease, despite the evident differences with human patients. At present, the best studied animal model of PD is the GAA-knockout murine model which lacks *Gaa* mRNA transcription and displays a virtually complete acid α-glucosidase deficiency. Such a model does not recapitulate the genetics of patients affected by late onset Pompe disease, in whom hypomorphic GAA mutations are present.

Zebrafish allows to recapitulate better the pathological human condition, characterized by the presence of mutated *gaa*, alongside with a variable amount of normal *gaa*.

The zebrafish provides an excellent model of normal and pathological muscle physiology, due to the conservation of protein-coding genes and organization and function of skeletal muscle between fish and humans. In the last 10 years, the zebrafish has become a prominent vertebrate model system for extensive analysis of gene function and signaling perturbation during development. The embryos are easy to handle and can be genetically manipulated by morpholino antisense oligonucleotide, mRNAs, transgenes, and genome editing techniques such as Clustered Regularly Interspersed Palindromic Repeats (CRISPR)-Cas9, Transcription Activator-Like Nucleases (TALENs), and Zinc Finger Nucleases (ZFNs).

Moreover, the relevance of this study lies on the possibility to lay the foundation to find a novel adjunct therapy for Pompe pathology.
In addition, zebrafish model will help to study the still unclear relation between glycogen storage and autophagy.
We believe that the zebrafish PD model will result in a suitable tool for different scientific fields, supporting investigation improvements in PD under many perspectives, including helping to shed light on impact of this pathology not only in heart, but also in the central nervous system.
In this study, we proposed to use 3-BrPA, an inhibitor of a key glycolytic enzyme (HK II), as a method to reduce the glucose uptake into the cell and to modulate autophagy in the muscular system. We are confident that 3-BrPA potentially represents a feasible treatment to improve quality of life and life expectancy in PD patients who have shown mild improvements with ERT.
Furthermore, we believe that the use of 3-BrPA, if efficacious in PD, could be extended to other disorders including Lafora disease which is characterized by glycogen accumulation in the brain and autophagy impairment.

3.2 Future prospects

In order to test longer 3-BrPA treatments and evaluate a longer effect on PD, we plan to generate a stable zebrafish *gaa* mutant carrying different GAA mutations, via the use of genome editing techniques. Such an animal model will be fundamental to reproduce the late onset human PD phenotype, and to demonstrate that long lasting 3-BrPA administration could really represent a new therapeutic strategy.
In order to generate the PD zebrafish stable mutant, we will take advantage of the transgenic line *Tg(CMV:EGFP-map1Lc3b),* generated by Klionsky laboratory in 2009 [134]. This line is characterized by the presence of the green fluorescent protein (GFP) under the Lc3b promoter, and allow the visualization of autophagosomes formation *in vivo*.

This transgenic line is already present in our zebrafish facility, kind gift of Dr. Annemarie H. Meijer from the Institute of Biology, Leiden University (Netherlands).

In order to generate the zebrafish PD mutants, we will use CRISPR–Cas systems, the most advanced technique applied to genome editing.

We will reproduce the human mutation c.1538A>G, p.Asp513Gly (p.D513G), which is present in homozygous in exon 10 of PD patients GAA. This novel variant, characterized by the replacement of glutamic acid with glycine at codon 513 of the GAA protein, is absent at least 240 control alleles based on whole exome database. Algorithms developed to predict the effect of the missense changes on protein structure and function, suggest that this variant is damaging/deleterious. In fact, the p.D513 residue has been reported to be important for post-translational modification and intracellular transport of GAA precursor [135].

The *in vitro* study reported in literature, showed that p.D513G did not interfere with the synthesis of the precursor protein, but disturbed protein processing and secretion. This variant displayed enzyme activity equivalent to negative control. Based on 3D structure available (PDB: 5NN8), the p.D513 residue is located at the N-terminus of the fourth beta-stand of the catalytic domain. The interactions of p. D513 which help to position the beta-strand and thus the catalytic acid/base, include salt bridge hydrogen bonds with p.H432 and p.R591 at the C-terminal ends of the second and fourth alpha-helices of the (beta/alpha)8 barrel. Therefore p.D513 has a crucial role in stabilizing the (beta/alpha)8 structure that is responsible for holding the two catalytic residues and the substrate in the exact position for hydrolysis. Replacing the Aspartic residue with Glycine will result in the loss of this charged H-bonding network, which should significantly destabilize this structure [136]

We are interested in this particular mutation because affects the amino acid asparagine (D), which is positioned 5 amino acids before the catalytic domain of the protein in human GAA. In zebrafish an asparagine is present in the same position as human protein sequence.

Human: -D-G-M-W-I-D-M-N-E-

Zebrafish: -D-G-L- W-I-D-M-N-E-

**in red, the Gaa catalytic domain; **highlighted in yellow the asparagine in position 513*

For this reason, we are confident that the generation of this mutant will recapitulate precisely the human pathological condition, and will be extremely important for the study of 3-BrPA effects.

3.3 Ongoing project on zebrafish transient PD model

Waiting for the authorization by the Italian Ministry of health, in order to proceed with the generation of mutant zebrafish PD model, we are testing an FDA approved drug on our zebrafish PD model, in collaboration with the company Catalyst Pharmaceuticals, Coral Gables, Florida.

This compound, named Amifampridine phosphate (3,4-DAPP), known under the trade name Firdapse, has been used to treat congenital myasthenic syndromes and Lambert–Eaton myasthenic syndrome (LEMS) since the 1990s.

The 3,4-DAPP blocks the potassium channel efflux in nerve terminals. Consequently, the action potential duration is increased, and the Ca^{2+} channels can stay open for a longer time and allow greater acetylcholine release to stimulate muscle at the end plate [137,138].

In literature, defects depending on neuromuscular junctions (NMJ) are reported in Pompe disease [139], as well as hypotheses to repair these hurdle with gene therapy [140].

Based on this assumption, we hypothesize to test the 3,4-DAPP, known to have effects on NMJ [141], in order to ameliorate the PD patients muscular condition.

Currently, we are investigating the effects of 3,4-DAPP administration on transient zebrafish PD model embryos, with a particular interest on NMJ. In fact, it is precisely on these structures that we are observing the main effects of the treatment, as expected.

Our results could allow the use of an already available drug, reducing timing and cost, to mitigate some secondary symptoms, as muscular fatigue and exhaustion, in Pompe disease.

POST SCRIPTUM

After this thesis was submitted to the reviewers, we have finished the experiments, wrote and submitted to Biomedicine & Pharmacotherapy journal the paper titled “Therapeutic efficacy of 3,4-Diaminopyridine phosphate on neuromuscular junction in Pompe disease”, by Bragato Cinzia, Blasevich Flavia, Ingenito Gary, Mantegazza Renato, Maggi Lorenzo.

Currently, we are working on the minor revisions required by the journal for publication.

3.4 Behind the 3-BrPA project

The idea underpinning the use of 3-BrPA as a treatment for Pompe disease was born during the last months of 2016.

At the end of a day spent in laboratory, I was reading the biography of some Nobel prize winners, when I came around the Dr. Otto Heinrich Warburg biography. For the discovery of the respiratory enzymes nature and mode of action, he won the Nobel Prize in 1931.

He became famous for his hypothesis on cancer growth, caused by tumor cells generating energy (as, e.g., adenosine triphosphate/ATP) mainly by anaerobic breakdown of glucose (known as fermentation, or anaerobic respiration). Warburg was the first to observe that, in tumor cells, the pyruvate, which is the last product of glycolysis, is converted into lactate, confirming the fact that even in aerobic conditions, cancer cells tend to favor metabolism via glycolysis. In oncology, this is known as the ‘Warburg effect’.

In the last 10 years, the research about 3-BrPA effects in these types of tumors, which basically incorporate glycogen to grow, has enormously increased.

Therefore, I started to be attracted by acid 3-bromopyruvic and its characteristics, and to hypothesize the possible use of this compound in other pathologies, as Pompe disease.

The idea to use a drug to reduce the entrance of glucose, in a system where the glycogen was already hugely stored, started to become interesting.

Soon after I have discussed every thought with Dr. Marina Mora, I've started to devise the experiments.

Moreover, we decided to propose the project to the Associazione Italiana Glicogenosi (AIG), in order to be funded. They believed on the validity of this research, and provided money for the material and for pay the zebrafish facility fee.

Few months later, I had the chance to compete for the PhD in Neuroscience with my project, and this gave me the possibility to continue my research experience.

I really hope that the present study on the use of 3-BrPA, could be just the beginning of a possible therapeutic strategy.

I hope to have the possibility to continue on this research, also after my PhD conclusion, in order to proceed on the test of 3-BrPA long lasting effects.

Nevertheless, I hope that also other research fields could be intrigued by the 3-BrPA potential in Pompe disease, in order to bring this research on a higher level.

Only together we will be able to find a remedy for Pompe disease patients, and consequently for their families.

Cinzia

Bibliografy

1. Cori GT. Biochemical aspects of glycogen deposition disease. *Bibl Paediatr* 1958;66:344-358.
2. De Duve C, Pressman BC, Gianetto R, Wattiaux R, Appelmans F. Tissue fractionation studies. 6. Intracellular distribution patterns of enzymes in rat-liver tissue. *Biochem J*. 1955;60:604-617.
3. Hers HG. alpha-Glucosidase deficiency in generalized glycogenstorage disease (Pompe's disease). *Biochem J*. 1963;86: 11-16.
4. Engel AG. Acid maltase deficiency in adults: studies in four cases of a syndrome which may mimic muscular dystrophy or other myopathies. *Brain.* 1970;93:599-616.
5. Lejeune N, Thines-Sempoux D, Hers HG. Tissue fractionation studies. 16. Intracellular distribution and properties of alpha-glucosidases in rat liver. *Biochem J* .1963;86:16-21.
6. Engel AG, Gomez MR, Seybold ME, Lambert EH. The spectrum and diagnosis of acid maltase deficiency. *Neurology*. 1973;23: 95-106.
7. Mechtler TP, Stary S, Metz TF, De Jesús VR, Greber-Platzer S, Pollak A et al. Neonatal screening for lysosomal storage disorders: feasibility and incidence from a nationwide study in Austria. *Lancet*. 2012;379:335-41.
8. Burton BK, Charrow J, Hoganson GE, Waggoner D, Tinkle B, Braddock SR et al. Newborn Screening for Lysosomal Storage Disorders in Illinois: The Initial 15-Month Experience. *J Pediatr*. 2017;190:130.
9. Chen LR, Chen CA, Chiu SN, Chien YH, Lee NC, Lin MT, et al. Reversal of cardiac dysfunction after enzyme replacement in patients with infantile-onset Pompe disease. *J Pediatr*. 2009;155:271–275.
10. Strothotte S, Strigl-Pill N, Grunert B, Kornblum C, Eger K, Wessig C, et al. Enzyme replacement therapy with alglucosidase alfa in 44 patients with late- onset glycogen storage disease type 2: 12-month results of an observational clinical trial. *J Neurol*. 2010;257:91–97.

11. Schoser B, Hill V, Raben N. Therapeutic approaches in glycogen storage disease type II/Pompe disease. Neurotherapeutics. 2008;5:569–578.
12. Kohler L, Puertollano R, Raben N. Pompe Disease: From Basic Science to Therapy. *Neurotherapeutics.* 2018;15:928-942.
13. Angelini C. Enzyme replacement therapy for the treatment of Pompe disease. Expert Opinion on Orphan Drugss. 2018;6:311-318.
14. Safary A, Akbarzadeh Khiavi M, Mousavi R, Barar J, Rafi MA. Enzyme replacement therapies: what is the best option? *Bioimpacts*. 2018;8:153-157.
15. Van den Hout H, Reuser AJ, Vulto AG, Loonen MC, Cromme-Dijkhuis A. Recombinant human alpha-glucosidase from rabbit milk in Pompe patients. *Lancet*. 2000;356:397-398.
16. Fiumara A. Enzyme replacement therapy (ERT) in Pompe disease. *Ital J Pediatr*. 2014;40(Suppl 1): A64.
17. Fukuda T, Roberts A, Ahearn M, Zaal K, Ralston E, Plotz PH, et al. Autophagy and lysosomes in Pompe disease. *Autophagy*. 2006;2: 318–320.
18. Thurberg BL, Lynch Maloney C, Vaccaro C, Afonso K, Tsai AC, Bossen PS, et al. Characterization of pre- and post-treatment pathology after enzyme replacement therapy for Pompe disease. *Lab Invest*. 2006;86:1208-1220.
19. Cardone M, Porto C, Tarallo A, Vicinanza M, Rossi B, Polishchuk E, et al. Abnormal mannose-6-phosphate receptor trafficking impairs recombinant alpha-glucosidase uptake in Pompe disease fibroblasts. *Pathogenetics*. 2008;1:6.
20. Van der Ploeg AT, Reuser AJJ. Pompe's disease. *Lancet.* 2008;372:1342–1353.
21. Mizushim, N. Autophagy, process and function. *Genes Dev*. 2007. 21;2861–2873.
22. Rubinsztein DC. Transcriptional regulation of mammalian autophagy at a glance. *J. Cell Sci*. 2016.129;3059–3066.

23. Khandia R, Dadar M, Munjal A, Dhama K, Karthik K, Tiwari R et al. A Comprehensive Review of Autophagy and Its Various Roles in Infectious, Non-Infectious, and Lifestyle Diseases: Current Knowledge and Prospects for Disease Prevention, Novel Drug Design, and Therapy. *Cell.* 2019; 8:674.
24. Mayer A. Determination of four sequential stages during microautophagy in vitro. *J. Biol. Chem*. 2004;279:9987–9996.
25. Li WW, Li J, Bao JK. Microautophagy, lesser-known self-eating. *Cell. Mol. Life Sci.* 2012;69:1125–1136.
26. Nakatogawa H, Suzuki K, Kamada Y, Ohsumi Y. Dynamics and diversity in autophagy mechanisms: lessons from yeast. *Nat. Rev. Mol. Cell Biol*. 2009;10: 458–467.
27. Rogov V, Dotsch V, Johansen T, Kirkin V. Interactions between autophagy receptors and ubiquitin-like proteins form the molecular basis for selective autophagy. *Mol. Cell*. 2014;53:167–178.
28. Lamark T, Svenning S, Johansen T. Regulation of selective autophagy: the p62/SQSTM1 paradigm. Essays in Biochem. 2017;61:609–624.
29. Paolini A, Omairi S, Mitchell R, Vaughan D, Matsakas A, Vaiyapuri S et al. Attenuation of autophagy impacts on muscle fibre development, starvation induced stress and fibre regeneration following acute injury. *Sci. Rep.* 2018.8; 9062.
30. Campbell P, Morris H, Schapira A. Chaperone-mediated autophagy as a therapeutic target for Parkinson disease. *Expert Opin. Ther. Targets.* 2018.22;823–832.
31. Qin ZH. (2019) Advances in Experimental Medicine and Biology. Autophagy: Biology and Diseases. Basic Science, Qin ZH Editor, Soochow University,Suzhou, China: Springer.
32. Yu L, Chena Y, Tooze SA. Autophagy pathway: Cellular and molecular mechanisms. *Autophagy*. 2018;2:207–215.
33. Klionsky DJ, Abdelmohsen K, Abe A, Abedin MJ, Abeliovich H, Acevedo Arozena A et al. Guidelines for the use and interpretation of

assays for monitoring autophagy (3rd edition). *Autophagy*. 2016;12(1):1-222.

34. Fodor E, T. Ari SE, Lengyel K, Takács-Vellai K, Varga M, Vellai T. Methods to Study Autophagy in Zebrafish. *Methods Enzymol*. 2017;588:467-496.
35. Kabeya Y, Mizushima N, Ueno T, Yamamoto A, Kirisako T, Noda T et al. LC3, a mammalian homologue of yeast Apg8p, is localized in autophagosome membranes after processing. *EMBO J*. 2000;19:5720-5728.
36. Tanida I, Ueno T, Kominami E. LC3 and Autophagy. *Methods Mol Biol*. 2008;445:77-88.
37. Aita VM, Liang XH, Murty VV, Pincus DL, Yu W, Cayanis E, Kalachikov S, Gilliam TC, Levine B. Cloning and genomic organization of beclin 1, a candidate tumor suppressor gene on chromosome 17q21. *Genomics*. 1999;59:59–65.
38. Tsujimoto Y, Cossman J, Jaffe E, CroceCM. Involvement of the bcl-2 gene in human follicular lymphoma. *Science*. 1985;228:1440–1443.
39. Liang XH, Jackson S, Seaman M, Brown K, Kempkes B, Hibshoosh H, Levine B Induction of autophagy and inhibition of tumorigenesis by beclin 1. *Nature*. 1999;402:672–676.
40. Ishii T, Yanagawa T, Yuki K, Kawane T, Yoshida H, Bannai S. Low micromolar levels of hydrogen peroxide and proteasome inhibitors induce the 60-kDa A170 stress protein in murine peritonealmacrophages. *Biochem Biophys Res Commun*. 1997;232: 33–37.
41. Alegre F, Moragrega AB, Polo M, Marti-Rodrigo A, Esplugues JV, Blas-Garcia A et al. Role of p62/SQSTM1 beyond autophagy: a lesson learned from drug-induced toxicity in vitro. *Br J Pharmacol*. 2018;175:440-455.
42. Bjørkøy G, Lamark T, Brech A, Outzen H, Perander M, Overvatn A, et al. p62/SQSTM1 forms protein aggregates degraded by autophagy and has a protective effect on huntingtin-induced cell death. *J Cell Biol*. 2005;171:603–614.

43. Puissant A, Fenouille N, Auberger P. When autophagy meets cancer through p62/SQSTM1. *Am J Cancer Res*. 2012;2:397–413.
44. Katsuragi Y, Ichimura Y, Komatsu M. p62/SQSTM1 functions as a signaling hub and an autophagy adaptor. *FEBS J.* 2015;282:4672–4678.
45. Maruyama T, Noda NN. Autophagy-regulating protease Atg4: structure, function, regulation and inhibition*. J Antibiot*. 2017;71:72-78
46. Wang JL, Wang JJ, Cai ZN, Xu CJ. The effect of curcumin on the differentiation, apoptosis and cell cycle of neural stem cells is mediated through inhibiting autophagy by the modulation of Atg7 and p62. *Int J Mol Med*. 2018;42:2481-2488.
47. Shimizu S. Biological Roles of Alternative *Autophagy.* Mol Cells. 2018;41:50-54.
48. Lin MG, Hurley JH. Structure and Function of the ULK1 Complex in Autophagy. *Curr Opin Cell Biol*. 2016;39:61-68.
49. Johansen T, Birgisdottir ÅB, Huber J, Kniss A, Dötsch V, Kirkin V et al. Methods for Studying Interactions Between Atg8/LC3/GABARAP and LIR-Containing Proteins. *Methods Enzymol*. 2017;587:143-169.
50. Schaaf MBE, Keulers TG, Vooijs MA, Rouschop KMA. LC3/GABARAP family proteins: autophagy-(un)related functions. *FASEB J*. 2016;30:3961-3978.
51. Papadopoli D, Boulay K, Kazak L, Pollak M, Mallette FA, Topisirovic I, et al. mTOR as a central regulator of lifespan and aging. *F1000Res*. 2019;8:F1000 Faculty Rev-998.
52. Switon K, Kotulska K, Janusz-Kaminska A, Zmorzynska J, Jaworski J. Molecular neurobiology of mTOR. Neuroscience. 2017;341:112-153.
53. Kim J, Kundu M, Viollet B, Guan KL. AMPK and mTOR regulate autophagy through direct phosphorylation of Ulk1. *Nat Cell Biol*. 2011;13:132-141.
54. Zhang CS, Jiang B, Li M, Zhu M, Peng Y, Zhang Y, et al. The lysosomal v-ATPase-Ragulator complex is a common activator for AMPK and mTORC1, acting as a switch between catabolism and anabolism. *Cell Metab*. 2014;20:526–540.

55. Spampanato C, Feeney E, Li L, Cardone M, Lim JA, Annunziata F et al. Transcription factor EB (TFEB) is a new therapeutic target for Pompe disease. *EMBO Mol. Med.* 2013.5;691–706.
56. Drost MR, Hesselink RP, Oomens CW, van der Vusse GJ. Effects of noncontractile inclusions on mechanical performance of skeletal muscle. *J. Biomech*. 2005.38;1035–1043.
57. Farah BL, Yen PM, Koeberl DD. Links between autophagy and disorders of glycogen metabolism–Perspectives on pathogenesis and possible treatments. *Mol Genet Metab*. 2020.129;3-12.
58. Meyer A1, Schartl M. Gene and genome duplications in vertebrates: the one-to-four (-to-eight in fish) rule and the evolution of novel gene functions. *Curr Opin Cell Biol*. 1999;11:699-704.
59. Taylor JS, Braasch I, Frickey T, Meyer A, Van de Peer Y. Genome duplication, a trait shared by 22000 species of ray-finned fish. *Genome Res*. 2003;13:382-390.
60. Howe K, Clark MD, Torroja CF, Torrance J, Berthelot C, Muffato M, et al. The zebrafish reference genome sequence and its relationship to the human genome. *Nature*. 2013;496(7446):498-503.
61. Lieschke GJ, Currie PD. Animal models of human disease: zebrafish swim into view. *Nat Rev Genet*. 2007;8:353-367.
62. Phillips JB, Westerfield M. Zebrafish models in translational research: tipping the scales toward advancements in human health. *Dis Model Mech*. 2014;7:739-743.
63. White RM. Cross-species oncogenomics using zebrafish models of cancer. *Curr Opin Genet Dev*. 2015;30:73-79.
64. Bradford YM, Toro S, Ramachandran S, Ruzicka L, Howe DG, Eagle A, et al. Zebrafish Models of Human Disease: Gaining Insight into Human Disease at ZFIN. *ILAR J.* 2017;58:4-16.
65. Postlethwait JH, Braasch I. In: The Zebrafish in Biomedical Research. Biology, Husbandry, Diseases, and Research Applications. Zebrafish Genetics – Chapter 3. American College of Laboratory Animal Medicine. Elsevier Inc., 2020.

66. Lin YY. Muscle diseases in the zebrafish. *Neuromuscul Disord.* 2012;22:673-684
67. Fleming A, Rubinsztein DC. Zebrafish as a model to understand autophagy and its role in neurological disease. *Biochim Biophys Acta*. 2011;1812:520-526.
68. Pistocchi A, Gaudenzi G, Foglia E, Monteverde S, Moreno-Fortuny A, Pianca A, et al. Conserved and divergent functions of Nfix in skeletal muscle development during vertebrate evolution. *Development.* 2013;140:1528-1536.
69. Stickney HL, Barresi MJ, Devoto SH. Somite development in zebrafish. *Dev Dyn.* 2000;219:287-303.
70. Coutelle O, Blagden CS, Hampson R, Halai C, Rigby PW, Hughes SM. Hedgehog signalling is required for maintenance of myf5 and myoD expression and timely terminal differentiation in zebrafish adaxial myogenesis. *Dev Biol*. 2001;236:136-50.
71. Devoto SH, Melançon E, Eisen JS, Westerfield M. Identification of separate slow and fast muscle precursor cells in vivo, prior to somite formation. *Development*. 1996;122:3371-3380.
72. Elworthy S, Hargrave M, Knight R, Mebus K, Ingham PW. Expression of multiple slow myosin heavy chain genes reveals a diversity of zebrafish slow twitch muscle fibres with differing requirements for Hedgehog and Prdm1 activity. *Development*. 2008;135:2115-2126.
73. Crawford BD, Henry CA, Clason TA, Becker AL, Hille MB. Activity and distribution of paxillin, focal adhesion kinase, and cadherin indicate cooperative roles during zebrafish morphogenesis. *Mol Biol Cell.* 2003;14:3065-3081.
74. Henry CA, Crawford BD, Yan YL, Postlethwait J, Cooper MS, Hille MB. Roles for zebrafish focal adhesion kinase in notochord and somite morphogenesis. *Dev Biol*. 2001;240:474-487.
75. Bassett DI, Bryson-Richardson RJ, Daggett DF, Gautier P, Keenan DG, Currie PD. Dystrophin is required for the formation of stable muscle attachments in the zebrafish embryo. *Development*. 2003;130:5851-5860.

76. Keenan SR, Currie PD. The Developmental Phases of Zebrafish Myogenesis. *J Dev Biol*. 2019;7(2).
77. Granato M, van Eeden FJ, Schach U, Trowe T, Brand M, Furutani-Seiki M, et al. Genes controlling and mediating locomotion behavior of the zebrafish embryo and larva. *Development*. 1996;123:399–413
78. Draper BW, Morcos PA, Kimmel CB. Inhibition of zebrafish fgf8 pre-mRNA splicing with morpholino oligos: a quantifiable method for gene knockdown. *Genesis*. 2001;30:154-156.
79. Sumanas S, Larson JD. Morpholino phosphorodiamidate oligonucleotides in zebrafish: a recipe for functional genomics? *Brief Funct Genomic Proteomic.* 2002;1:239-256.
80. Zhang Q, Zhang Y, Zhang P, Chao Z, Xia F, Jiang C, Zhang X, Jiang Z, Liu H. Hexokinase II inhibitor, 3-BrPA induced autophagy by stimulating ROS formation in human breast cancer cells. *Genes & Cancer.* 2014;5:3-4.
81. Pelicano H, Martin DS, Xu R-H, Huang P. Glycolysis inhibition for anticancer treatment. *Oncogene*. 2006; 25:4633–4646.
82. Graziano F, Ruzzo A, Giacomini E, Ricciardi T, Aprile G, Loupakis F, et al. Glycolysis gene expression analysis and selective metabolic advantage in the clinical progression of colorectal cancer. *Pharmacogenomics J*. 2016;1-7.
83. Geschwind JH, Ko YH, Torbenson MS, Magee C, Pedersen PL. Novel Therapy for Liver Cancer: Direct Intraarterial Injection of a Potent Inhibitor of ATP. *Cancer Research*. 2002;62:3909- 3913.
84. Ganapathy-Kanniappan S, Geschwind JF, Kunjithapatham R, Buijs M, Syed LH, Rao PP, et al. 3-Bromopyruvate induces endoplasmic reticulum stress, overcomes autophagy and causes apoptosis in human HCC cell lines. *Anticancer Res*. 2010;30:923-935
85. Davidescu M, Sciaccaluga M, Macchioni L, Angelini R, Lopalco P, Rambotti MG, et al. Bromopyruvate mediates autophagy and cardiolipin degradation to monolyso-cardiolipin in GL15 glioblastoma cells. *J Bioenerg Biomembr*. 2012;44:51-60.

86. Tsai HJ, Wilson JE. Functional organization of mammalian hexokinases: both N- and C-terminal halves of the rat type II isozyme possess catalytic sites. *Arch Biochem Biophys*. 1996;329:17–23.
87. Ko YH, Pedersen PL, Geschwind JF. Glucose catabolism in the rabbit VX2 tumor model for liver cancer: characterization and targeting hexokinase. *Cancer Lett*. 2001;173:83–91.
88. Pedersen PL Warburg, me and Hexokinase 2: Multiple discoveries of key molecular events underlying one of cancers' most common phenotypes, the "Warburg Effect", i.e., Elevated glycolysis in the presence of oxygen. *J Bioenerg Biomembr*. 2007;39:211–222.
89. Queiros O, Preto A, Pacheco A, Pinheiro C, Azevedo-Silva J, Moreira R, et al. Butyrate activates the monocarboxylate transport- er MCT4 expression in breast cancer cells and enhances the antitumor activity of 3-bromopyruvate. *J Bioenerg Biomembr*. 2012;44:141–153.
90. Halestrap AP, Price NT. The proton-linked monocarboxylate transporter (MCT) family: structure, function and regulation. *Biochem. J*. 1999;343:281–299.
91. Macchioni L, Davidescu M, Roberti R, Corazzi L. The energy blockers 3-bromopyruvate and lonidamine: effects on bioenergetics of brain mitochondria. *J Bioenerg Biomembr*. 2014;46:389–394.
92. Azevedo-Silva J, Queirós O, Baltazar F, Ułaszewski S, Goffeau A, Ko YH, et al. The anticancer agent 3-bromopyruvate: a simple but powerful molecule taken from the lab to the bedside. *J Bioenerg Biomembr.* 20164;8:349–362
93. González-Alvarez R, Ortega-Cuellar D, Hernández-Mendoza A, Moreno-Arriola E, Villaseñor-Mendoza K, Gálvez-Mariscal A. The hexokinase gene family in the zebrafish: structure, expression, functional and phylogenetic analysis. *Comp Biochem Physiol B Biochem Mol Biol.* 2009;152:189-195.
94. Omlin T, Weber JM. Exhausting exercise and tissue-specific expression of monocarboxylate transporters in rainbow trout. *Am J Physiol Regul Integr Comp Physiol.* 2013;304:R1036-1043.

95. Güngör D, Reuser AJJ. How to describe the clinical spectrum in Pompe disease? *Am J Med Genet*. 2013;161:399–400.
96. Raben N, Danon M, Gilbert AL, Dwivedi S, Collins B, Thurberg BL, et al. Enzyme replacement therapy in the mouse model of Pompe disease. *Mol Genet Metab*. 2003;80:159–169.
97. Van den Hout JM, Kamphoven JH, Winkel LP, Arts WF, De Klerk JB, Loonen MC, et al. Long-term intravenous treatment of Pompe disease with recombinant human alpha-glucosidase from milk. *Pediatrics*. 2004;113:448–457.
98. Levine B and Klionsky DJ. Development by self-digestion: molecular mechanisms and biological functions of autophagy. *Dev Cell*. 2004;6:463–477.
99. Mizushima N, Levine B. Autophagy in mammalian development and differentiation. *Nat Cell Biol*. 2010;12:823–830.
100. Lee DL, Bareja A, Bartlett DB, White JP. Autophagy as a Therapeutic Target to Enhance Aged Muscle Regeneration. *Cells*. 2019;8:183.
101. Raben N, Roberts A, Plotz PH. Role of autophagy in the pathogenesis of Pompe disease. *Acta Myol.* 2007;26:45-48.
102. Kishnani PS and Beckemeyer AA. New therapeutic approaches for Pompe disease: enzyme replacement therapy and beyond. *Pediatr Endocrinol Rev*. 2014;1:114-124.
103. McCall AL, Stankov SG, Cowen G, Cloutier D, Zhang Z, Yang L, et al. Reduction of Autophagic Accumulation in Pompe Disease Mouse Model Following Gene Therapy. *Curr Gene Ther*. 2019;19(3):197-207.
104. Lim JA, Yi H, Gao F, Raben N, Kishnani PS, Sun B. Intravenous Injection of an AAV-PHP.B Vector Encoding Human Acid α-Glucosidase Rescues Both Muscle and CNS Defects in Murine Pompe Disease. *Mol Ther Methods Clin Dev*. 2019;12: 233–245.
105. Takikita S, Schreiner C, Baum R, Xie T, Ralston E, Plotz PH, et al. Fiber Type Conversion by PGC-1α Activates Lysosomal and Autophagosomal Biogenesis in Both Unaffected and Pompe Skeletal Muscle. *PLoS One*. 2010;5(12):e15239.

106. Martina JA, Diab HI, Lishu L, Jeong-A L, Patange S, Raben N, et al. The Nutrient-Responsive Transcription Factor TFE3, Promotes Autophagy, Lysosomal Biogenesis, and Clearance of Cellular Debris. *Sci Signal*. 2014;7(309): ra9.
107. Raben N, Nagaraju K, Lee E, Kessler P, Byrne B, Lee L, et al. Targeted Disruption of the Acid α-Glucosidase Gene in Mice Causes an Illness with Critical Features of Both Infantile and Adult Human Glycogen Storage Dis. Type II. *J Biol Chem*. 1998; 73(30):19086-19092.
108. Hiniker A, Margeta M. Skeletal myopathy in Pompe disease: a failure of satellite cell activation? Acta Neuropathol Commun. 2018; 6(1):133.
109. Varga M, Fodor E, Vellai T. Autophagy in zebrafish. *Methods*. 2015;75:172-180.
110. Mathai BJ, Meijer AH, Simonsen A. Studying Autophagy in Zebrafish. *Cells*. 2017;6(3):E21.
111. González-Alvarez R, Ortega-Cuellar D, Hernández-Mendoza A, Moreno-Arriola E, Villaseñor-Mendoza K, Gálvez-Mariscal A, et al. The hexokinase gene family in the zebrafish: Structure, expression, functional and phylogenetic analysis. *Comp Biochem Physiol B Biochem Mol Biol.* 2009;152(2):189-195.
112. Nasevicius A, Ekker SC. Effective targeted gene 'knockdown' in zebrafish. *Nat Genet*. 2000;26:216–220.
113. Kimmel CB, Ballard WW, Kimmel ST, Ullmann B, Schilling TF. Stages of Embryonic Development of the Zebrafish. *Dev Dyn*. 1995;203:253-310.
114. He C, Klionsky DJ. Analyzing autophagy in zebrafish. *Autophagy*. 2010;6:642-644.
115. Schindelin J, Arganda-Carreras I, Frise E, Kaynig V, Longair M, Pietzsch T, et al. Fiji: an open-source platform for biological-image analysis. *Nat Methods*. 2012;9:676–682.
116. Ro H, Soun K, Kim E, Rhee M. Novel Vector System Opimized for injecting in vitro-synthetized mRNA into zebrafish embryos. *Mol Cells*. 2004;17:373-376.

117. Shoshan MC. 3-bromopyruvate: Targets and outcomes. *J Bioenerg Biomembr*. 2012;44:7-15.
118. Louzao MC, Espiña B, Vieytes MR, Vega FV, Rubiolo JA, Baba O, et al. ”Fluorescent glycogen" formation with sensibility for in vivo and in vitro detection. *Glycoconj J*. 2008;25(6):503-510.
119. Dasouki M, Jawdat O, Almadhoun O, Pasnoor M, McVey ML, Abuzinadah A, et al. Pompe disease: Literature Review and Case Series. *Neurol Clin*. 2014;32:751-779.
120. Tabassum N, Tai H, Jung D, Williams DR. Fishing for Nature’s Hits: Establishment of the Zebrafish as a Model for Screening Antidiabetic Natural Products. *Evid Based Complement Alternat Med*. 2015;2015:287847.
121. Lockhart M, Wirrig E, Phelps A, Wessels A. Extracellular Matrix and Heart Development. *Birth Defects Res A Clin Mol Teratol*. 2011;91:535-550.
122. Forsha D, Li JS, Smith PB, van der Ploeg AT, Kishnani P, Pasquali SK. Cardiovascular Abnormalities in Late Onset Pompe disease and Response to Enzyme Replacement Therapy for the Late Onset Treatment Study Investigators. *Genet Med*. 2011;13:625-631.
123. Ravikumar B, Sarkar S, Davies JE, Futter M, Garcia-Arencibia M, Green-Thompson ZW, et al. Regulation of mammalian autophagy in physiology and pathophysiology. *Physiol Rev*. 2010;90:1383-1435.
124. Agnello M, Bosco L, Chiarelli R, Martino C, Roccheri MC. The role of autophagy and apoptosis during embryo development. In Ntuli TM, eds. Cell Death – Autophagy, Apoptosis and Necrosis. Rijeka: Croatia: INTECH Press; 2015:83–112.
125. Miccoli A, Dalla Valle L, Carnevali O. The maternal control in the embryonic development of zebrafish. *Gen Comp Endocrinol*. 2017;245:55-58.
126. Kang R, Zeh HJ, Lotze MT, Tang D. The Beclin 1 network regulates autophagy and apoptosis. *Cell Death Differ*. 2011;18:571-580.

127. Liu WJ, Ye L, Huang WF, Guo LJ, Xu ZG, Wu HL, et al. p62 links the autophagy pathway and the ubiqutin-proteasome system upon ubiquitinated protein degradation. *Cell Mol Biol Lett*. 2016;21:29.
128. McManus J, Cheng Z, Vogel C. Next-generation analysis of gene expression regulation–comparing the roles of synthesis and degradation. *Mol Biosyst*. 2015;11:2680–2689.
129. Jiao L, Zhang HL, Li DD, Yang KL, Tang J, Li X, et al. Regulation of Glycolytic Metabolism by Autophagy in Liver Cancer Involves Selective Autophagic Degradation of HK2 (hexokinase 2). *Autophagy*. 2018;14:671-684.
130. Birsoy K, Wang T, Possemato R, Yilmaz OH, Koch CE, Chen WW, et al. MCT1-mediated transport of a toxic molecule is an effective strategy for targeting glycolytic tumors. *Nat Genet*. 2013;45:104–110.
131. Ehrke E, Arend C, Dringen R. 3-Bromopyruvate Inhibits Glycolysis, Depletes Cellular Glutathione, and Compromises the Viability of Cultured Primary Rat Astrocytes. *J Neurosci Res*. 2015;93:1138-1146.
132. Xu H, Ren D. Lysosomal Physiology. *Annu Rev Physiol*. 2015;77:57-80.
133. Wu J, Yang Y, Sun C, Sun S, Li Q, Yao Y, et al. Disruption of the gaa Gene in Zebrafish Fails to Generate the Phenotype of Classical Pompe Disease. *DNA and cell biol*. 2017;36:10–17.
134. He C, Bartholomew CR, Zhou W, Klionsky DJ. Assaying autophagic activity in transgenic GFP-Lc3 and GFP-Gabarap zebrafish embryos. *Autophagy*. 2009;5:520-526.
135. Hermans MM, De Graaff E, Kroos MA, Mohkamsing S, Eussen BJ, Joosse M, et al. The effect of a single base pair deletion (delta T525) and a C1634T missense mutation (pro545leu) on the expression of lysosomal alpha-glucosidase in patients with glycogen storage disease type II. *Hum Mol Genet.* 1994;3:2213-2218.
136. Ngiwsara L, Wattanasirichaigoon D, Tim-Aroon T, Rojnueangnit K, Noojaroen S, Khongkraparn A, et al. Clinical course, mutations and its

functional characteristics of infantile-onset Pompe disease in Thailand. *BMC Med Genet*. 2019;20:156.

137. Kirsch GE, Narahashi T. 3,4-diaminopyridine. A potent new potassium channel blocker. *Biophys J*. 1978;22:507–512.
138. Tarr TB, Wipf P, Meriney ST. Synaptic pathophysiology and treatment of Lambert-Eaton myasthenic syndrome. *Mol Neurobiol*. 2015;52: 456–463.
139. Falk DJ, Todd AG, Lee S, Soustek MS, ElMallah MK, Fuller DD, et al. Peripheral nerve and neuromuscular junction pathology in Pompe disease. *Hum Mol Genet*. 2015;24:625-636.
140. Todd AG, McElroy JA, Grange RW, Fuller DD, Walter GA, Byrne BJ, et al. Correcting Neuromuscular Deficits With Gene Therapy in Pompe Disease. *Ann Neurol.* 2015;78:222-234.
141. Vazquez-Cintron E, Machamer J, Ondeck C, Pagarigan K, Winner B, Bodner P, et al. Symptomatic treatment of botulism with a clinically approved small molecule. *JCI Insight*. 2020;5(2).